Journal of Medicinal Chemistry

pubs.acs.org/jmc

Article

# Potent Anti-SARS-CoV-2 Activity by the Natural Product Gallinamide A and Analogues via Inhibition of Cathepsin L

Anneliese S. Ashhurst, Arthur H. Tang, Pavla Fajtová, Michael C. Yoon, Anupriya Aggarwal, Max J. Bedding, Alexander Stoye, Laura Beretta, Dustin Pwee, Aleksandra Drelich, Danielle Skinner, Linfeng Li, Thomas D. Meek, James H. McKerrow, Vivian Hook, Chien-Te Tseng, Mark Larance, Stuart Turville, William H. Gerwick,* Anthony J. O'Donoghue,* and Richard J. Payne*

Cite This: https://doi.org/10.1021/acs.jmedchem.1c01494

Read Online

ACCESS | Metrics & More | Article Recommendations | Supporting Information

**ABSTRACT:** Cathepsin L is a key host cysteine protease utilized by coronaviruses for cell entry and is a promising drug target for novel antivirals against SARS-CoV-2. The marine natural product gallinamide A and several synthetic analogues were identified as potent inhibitors of cathepsin L with $IC_{50}$ values in the picomolar range. Lead molecules possessed selectivity over other cathepsins and alternative host proteases involved in viral entry. Gallinamide A directly interacted with cathepsin L in cells and, together with two lead analogues, potently inhibited SARS-CoV-2 infection *in vitro*, with $EC_{50}$ values in the nanomolar range. Reduced antiviral activity was observed in cells overexpressing transmembrane protease, serine 2 (TMPRSS2); however, a synergistic improvement in antiviral activity was achieved when combined with a TMPRSS2 inhibitor. These data highlight the potential of cathepsin L as a COVID-19 drug target as well as the likely need to inhibit multiple routes of viral entry to achieve efficacy.

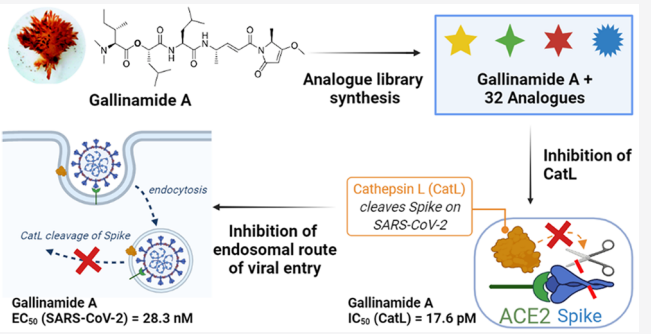


## INTRODUCTION

The novel severe acute respiratory syndrome (SARS)-like coronavirus-2 (SARS-CoV-2) is a beta-coronavirus responsible for COVID-19, a respiratory disease that emerged from the Hubei province in China in December 2019 and was declared a global pandemic on the 11th of March 2020.[1] Alarmingly, in less than 18 months, COVID-19 has been reported in nearly every country, with over 237 million confirmed COVID-19 cases and more than 4.8 million deaths globally (at the time of writing). The COVID-19 pandemic has had a devastating effect on both global health and the functioning of society, and prophylactic and therapeutic intervention strategies are urgently needed. To date, there has been an intense global effort directed toward the development of an effective COVID-19 vaccine, with several candidates,[2] including two mRNA vaccines and a chimpanzee adenovirus-vectored vaccine, completing phase III human clinical trials[3−5] and now in widespread use globally. In addition to an effective prophylactic vaccine, the control of COVID-19, and potentially future SARS coronavirus zoonoses, also requires efficacious antiviral therapeutics, particularly in light of the rapid emergence of variant strains.

While antiviral drug discovery for SARS-CoV-2 has been the subject of significant effort, the majority of molecules currently in clinical trials are repurposed from other indications for which they were originally approved. Remdesivir is currently the only antiviral drug to be approved by the United States Food and Drug Administration (FDA) for the treatment of COVID-19. While this molecule has been reported to show some efficacy during early infection, the drug has performed poorly in a number of trials where it was deemed ineffective,[6,7] including a recent report from the World Health Organization that suggested remdesivir provided little to no effect in the outcome of COVID-19 infections in hospitalized patients.[8] Examples of other repurposing approaches that have been explored include the use of hydroxychloroquine,[9−11] the HIV therapy lopinavir−ritonavir,[12,13] as well as type I interferon regimens;[14,15] however, these too have shown no improvement over standard care in hospitalized COVID-19 patients. At the present time, one of the most effective means of improving COVID-19 patient outcomes has been through the use of the glucocorticoid dexamethasone, which serves to reduce inflammation-mediated lung injury.[16] Taken together, despite

Special Issue: COVID-19

Received: August 24, 2021

significant effort from the global research community, there is still an urgent need to discover effective antivirals for COVID-19 infection that operate through novel mechanisms of action and that are distinctive to the molecules currently in use. While there are obvious benefits to postexposure drug therapies, the development of a pre-exposure prophylaxis approach, such as what has been employed for HIV,[17] would also be transformative for protecting vulnerable communities.

SARS-CoV-2 shares 82% genome identity to the SARS-CoV that emerged in Guangdong province, China, in 2002. It is now accepted that the two coronaviruses share similar molecular mechanisms of host cell recognition, entry, and replication.[18−20] Recognition and entry of SARS-CoV-2 into target cells relies on binding between the receptor-binding domain (RBD) of an envelope homotrimeric spike glycoprotein (S) and the host cellular receptor, angiotensin-converting enzyme 2 (ACE2) (Figure 1A). Recently, a second receptor protein, a transmembrane glycoprotein of the immunoglobulin superfamily known as CD147, has been identified as mediating spike protein interaction and viral uptake via endocytosis.[21] Each monomeric unit of the S protein contains an S1 and S2 subunit that mediate attachment and membrane fusion with host cells, respectively. Host cell entry requires priming of the S protein by cleavage at the S1/S2 and the S2′ site that enables fusion of viral and cellular membranes. This cleavage has been shown to be carried out primarily by the membrane-bound serine protease TMPRSS2[19] but can also be performed by the cysteine protease, cathepsin L (CatL).[22,23] Following entry of the virus into the cell via an endosomal pathway, CatL is responsible for S1 cleavage at acidic pH, conditions where TMPRSS2 is not catalytically functional. Overexpression of CatL in human cell lines enhances SARS-CoV-2 spike-mediated viral entry, while circulating CatL is elevated during COVID-19 disease and correlates with progression and severity.[24] Finally, it is known that expression of CatL, but not cathepsin B (CatB), is upregulated by interleukin-6 (IL-6).[25] This is of importance, as there is early evidence that IL-6 is a surrogate inflammatory marker for severe COVID-19 disease with poor prognosis.[26] This would imply that CatL is upregulated under these conditions and would therefore be a potentially important target for controlling excessive pathology.

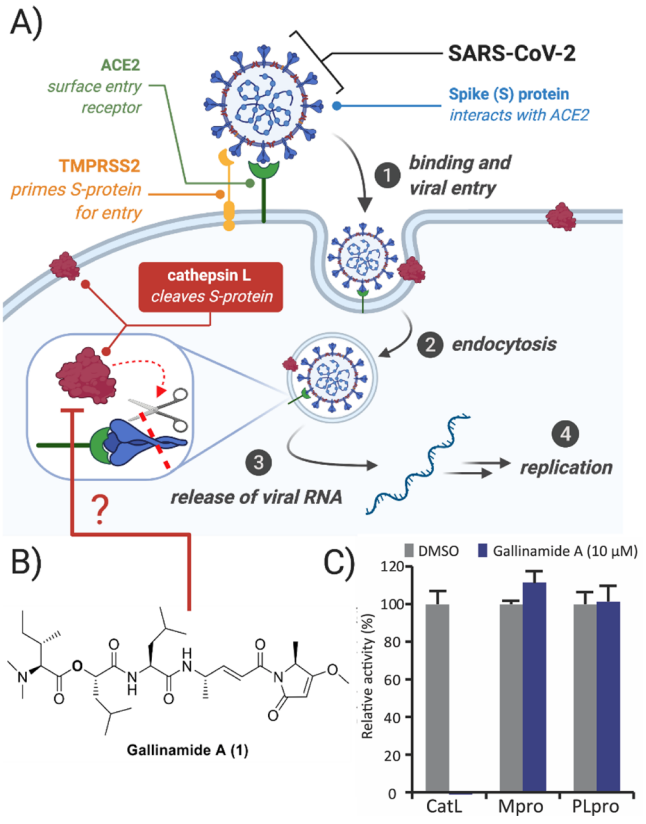


**Figure 1.** Targeting cathepsin L with gallinamide A to inhibit SARS-CoV-2. (A) Role of host proteases in cell entry mechanisms for SARS-CoV-2 (endocytic entry route shown, NB: TMPRSS2 primes S-protein for nonendocytic entry). (B) Structure of the natural product depsipeptide CatL inhibitor gallinamide A (**1**). (C) Enzymatic activity of CatL, Mpro, and PLpro following incubation with 10 $\mu$M gallinamide A. Assays were performed in triplicate wells, data are the means +/- SD, and relative activity was compared to reactions containing 0.2% DMSO.

This dual role of CatL in the establishment and progression of COVID-19 pathology has therefore reinforced the enzyme as a key drug target for SARS-CoV-2.[27] The importance of both TMPRSS2 and CatL for facilitating viral entry and replication is highlighted by the effectiveness of TMPRSS2 inhibitors camostat mesylate[19] and nafamostat mesylate[28] and the pan-cysteine protease inhibitors E64d[19] and K777[23] to reduce virus infection levels of SARS-CoV-2 (and SARS-CoV) in a range of human cell lines. Following uncoating and release of the viral RNA from the endosome, translation of the two large viral reading frames gives rise to the polyproteins pp1a and pp1ab that are subsequently processed by two viral proteases: the main protease (Mpro) and the papain-like protease (PLpro).[18] This gives rise to a number of nonstructural proteins that subsequently orchestrate viral replication and release from infected cells to infect new cells. As such, both Mpro and PLpro are also promising antiviral targets for SARS-CoV-2.[29−32]

Gallinamide A **1** (also known as symplostatin 4) is a modified depsipeptide natural product that was independently discovered from marine cyanobacteria of the *Schizothrix* genus in Panama[33] and *Symploca* in Florida.[34] The natural product has several unusual structural features, including a pyrrolinone derived from L-alanine and an $\alpha,\beta$-unsaturated imide moiety (Figure 1B). Notably, gallinamide A has been demonstrated to be a potent covalent inhibitor of several parasite-derived cysteine proteases,[35−37] as well as human CatL,[38] with several synthetic analogues of the natural product also shown to have potent *in vivo* antimalarial activity in a murine model.[39] Given the importance of CatL for cellular entry of SARS-CoV-2, we investigated whether the CatL inhibitory activity of gallinamide A could be leveraged for SARS-CoV-2 antiviral activity. Toward this end, we assembled an international consortium to investigate gallinamide A, together with 32 synthetic natural product analogues, as novel inhibitors of SARS-CoV-2 entry. We report herein that several analogues exhibit potent inhibitory activity against CatL with $IC_{50}$ values in the low nanomolar to picomolar range. Several of these gallinamide A-inspired molecules also possess selectivity over CatB and other related cathepsin proteases and do not inhibit the two viral proteases Mpro and PLpro, or host cell proteases furin and TMPRSS2. We demonstrate that gallinamide A and two of the most active CatL-inhibiting natural product analogues potently inhibit SARS-CoV-2 infection *in vitro*, with $EC_{50}$ values in the nanomolar range. In TMPRSS2


https://doi.org/10.1021/acs.jmedchem.1c01494
J. Med. Chem. XXXX, XXX, XXX−XXX

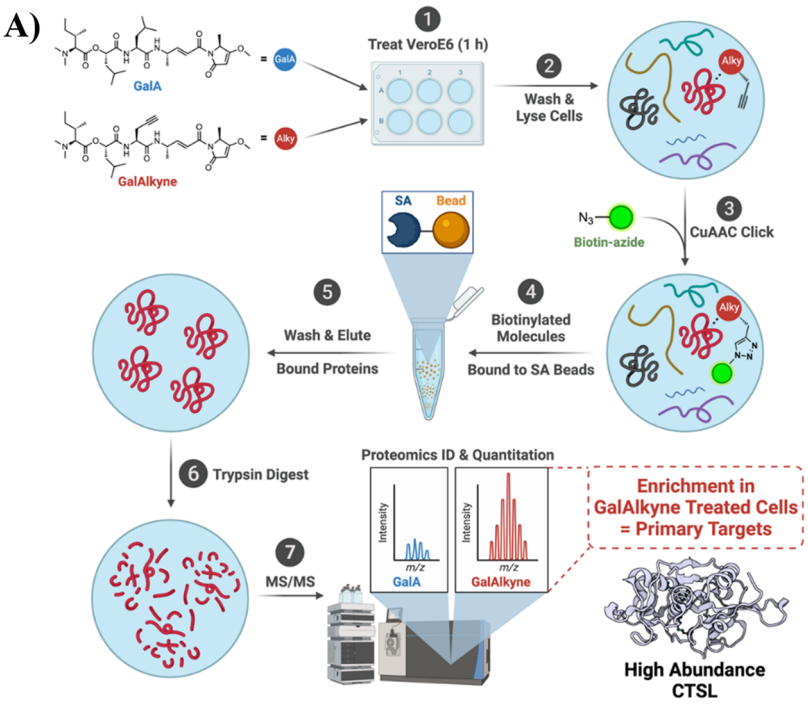


B)

Log10(iBAQ Intensity) 5.000 – 10.000

| | | GalA | | | GalA Alkyne | | | Enrichment (GalA-Alkyne /GalA) |
|---|---|---|---|---|---|---|---|---|
| A0A0D9R4W3 | Cathepsin L | 6.4 | 6.4 | 7.2 | 9.7 | 9.8 | 9.9 | 1293 |
| A0A0D9RWL1 | Cathepsin B | | | 6.4 | 8.8 | 8.8 | 8.8 | 279 |
| A0A0D9RST9 | Cathepsin X | | | 5.4 | 7.9 | 7.8 | 7.9 | 299 |
| A0A0D9S0P4 | Cathepsin C | | | | 7.7 | 7.6 | 7.6 | - |
| A0A0D9RZM0 | Cathepsin K | | | | 7.7 | 7.7 | 7.7 | - |
| A0A0D9R7K9 | Cathepsin F | | | | 7.1 | 7.1 | 6.7 | - |
| A0A0D9S1Q7 | Cathepsin O | | | | 7.0 | | 7.1 | - |
| A0A0D9RBZ8 | Cathepsin D | 6.0 | | 6.1 | 6.3 | 6.6 | 6.5 | 3 |

**Figure 2.** Identification of gallinamide A targets in VeroE6 cells. (A) Schematic overview of the experiment. VeroE6 cells were incubated for 1 h with 10 $\mu$M of either gallinamide A **1** (GalA, negative control) or gallinamide A-alkyne (GalAlkyne, test, $k_{inact}/K_I^{app}$ = (9.91 ± 2.11) × $10^3$ $s^{-1}$ $M^{-1}$ for inhibition of human CatL with ± SD for four technical replicates). Lysate proteins underwent a Cu(I)-catalyzed click reaction to biotin-azide, prior to enrichment on streptavidin beads. Proteins bound to the beads were quantified by mass spectrometry-based proteomics using the iBAQ intensity, which normalizes for the ability of each protein to generate LC-MS/MS compatible tryptic peptides. Cathepsin L (CTSL, structure PDB code: 3HHA). (B) The $Log_{10}$(iBAQ intensity) for the major cellular cathepsins detected in each biological replicate ($n$ = 3) are indicated one per cell as a heat map, with a color gradient and a label showing the $log_{10}$ value. Heat map cells without a value indicate no detection. The Uniprot identifier and name are indicated for each protein. The fold-change enrichment for GalAlkyne over GALA is indicated in the right-hand column and used the average value for each protein across the replicates. Enrichments are not reported for Cathepsin C, K, F, and O because these proteins were not detected in the GalA negative control sample.

overexpressing cells, a setting in which there are compensatory viral entry mechanisms, the antiviral activity of gallinamide A was reduced; however, there was a synergistic improvement in activity when combined with the TMPRSS2 inhibitor nafamostat mesylate. These data highlight the potential of CatL as a COVID-19 antiviral target and the likely importance of targeting multiple entry mechanisms through drug combinations for effective COVID-19 treatment.

## RESULTS

**Gallinamide A Inhibits SARS-CoV-2 Infection *in Vitro* via the Inhibition of CatL.** Gallinamide A (**1**) was initially screened in a SARS-CoV-2 viral infection assay in Vero 76 clone E6 cells (VeroE6) at the National Institute of Allergy and Infectious Disease (NIAID) to gauge whether the natural product exhibited antiviral activity. Pleasingly, gallinamide A was shown to decrease viral load with an $IC_{90}$ of 88 nM. Following this, we further validated the activity of the natural product by performing the *in vitro* SARS-CoV-2 infectivity assay in our own laboratories using VeroE6 cells and adenocarcinomic human alveolar basal epithelial cells over-expressing ACE2 (A549/ACE2). Briefly, gallinamide A (**1**) was preincubated with 4000 VeroE6 cells in a 384-well plate for 30 min and then challenged with 0.5 MOI SARS-CoV-2. In the absence of treatment, these conditions lead to viral cytopathic effects (CPE) and cell loss that is correlated to the level of available infectious virus in the initial inoculum after 72 h. Addition of inhibitors that block viral entry reduces CPE/cell loss in a dose-dependent manner. To obtain a quantitative measure of CPE, the nuclei of live cells were stained, imaged and enumerated using high-content image analysis software. Using this method, we could readily generate dose-dependent sigmoidal inhibition curves and calculated an $EC_{50}$ of 28 ± 12 nM for gallinamide A from


https://doi.org/10.1021/acs.jmedchem.1c01494
J. Med. Chem. XXXX, XXX, XXX−XXX

A)

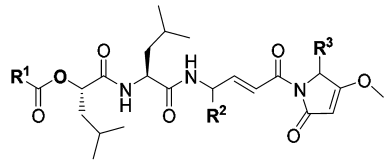

1-10

| Compound | $R^1$ | $R^2$ | $R^3$ |
|---|---|---|---|
| 1 | *N,N*-$Me_2$-L-Ile | (*S*)-$CH_3$ | (*S*)-$CH_3$ |
| 2 | *N,N*-$Me_2$-L-Phe | (*S*)-$CH_3$ | (*S*)-$CH_2Ph$ |
| 3 | *N,N*-$Me_2$-L-Ile | (*S*)-$CH_3$ | (*S*)-$CH_2CH(CH_3)_2$ |
| 4 | *N,N*-$Me_2$-L-Val | (*S*)-$CH_3$ | (*S*)-$CH_3$ |
| 5 | *N,N*-$Me_2$-L-Phe | (*S*)-$CH_2Ph$ | (*S*)-$CH_3$ |
| 6 | *N,N*-$Me_2$-L-Phe | (*S*)-$CH_2Ph$ | (*R*)-$CH_2Ph$ |
| 7 | *N,N*-$Me_2$-L-Ile | (*S*)-$CH_2Ph$ | (*S*)-$CH_2Ph$ |
| 8 | *N,N*-$Me_2$-L-Phe | (*S*)-$CH_2Ph$ | (*S*)-$CH_2Ph$ |
| 9 | *N,N*-$Me_2$-L-Ile | (*R*)-$CH_2Ph$ | (*S*)-$CH_2Ph$ |
| 10 | *N,N*-$Me_2$-L-Ile | (*R*)-$CH_2Ph$ | (*R*)-$CH_2Ph$ |

B)

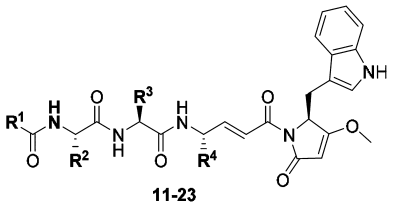

11-23

| Compound | $R^1$ | $R^2$ | $R^3$ | $R^4$ |
|---|---|---|---|---|
| 11 | *N,N*-$Me_2$-L-Val | $CH_2CH(CH_3)_2$ | $CH_2CH(CH_3)_2$ | $CH_3$ |
| 12 | *N,N*-$Me_2$-L-Val | $CH_2$cyclohexyl | $CH_2$cyclohexyl | $CH_3$ |
| 13 | *N,N*-$Me_2$-L-Val | $CH_2CH(CH_3)_2$ | $CH_2$cyclohexyl | $CH_3$ |
| 14 | *N,N*-$Me_2$-L-Val | $CH_2$cyclohexyl | $CH_2CH(CH_3)_2$ | $CH_3$ |
| 15 | *N,N*-$Me_2$-L-Val | $CH_2CH(CH_3)_2$ | $CH_2CH_2Ph$ | $CH_3$ |
| 16 | 4-(*N*-Me)piperidine | $CH_2CH(CH_3)_2$ | $CH_2$cyclohexyl | $CH_3$ |
| 17 | 4-(*N*-Me)piperidine | $CH_2$cyclohexyl | $CH_2CH(CH_3)_2$ | $CH_3$ |
| 18 | 4-(*N*-Me)piperidine | $CH_2$cyclohexyl | $CH_2$cyclohexyl | $CH_3$ |
| 19 | *N,N*-$Me_2$-L-Val | $CH_2$cyclohexyl | $CH_2CH_2Ph$ | $CH_3$ |
| 20 | 4-(*N*-Me)piperidine | $CH_2CH(CH_3)_2$ | $CH_2CH(CH_3)_2$ | $CH_3$ |
| 21 | *N,N*-$Me_2$-L-Val | $CH_2Ph$ | $CH_2CH(CH_3)_2$ | $CH_3$ |
| 22 | *N,N*-$Me_2$-L-Val | $CH_2$cyclohexyl | $CH_2CH(CH_3)_2$ | Cyclohexyl |
| 23 | *N,N*-$Me_2$-L-Val | $CH_2CH(CH_3)_2$ | $CH_2CH(CH_3)_2$ | $CH_2CH_2Ph$ |

C)

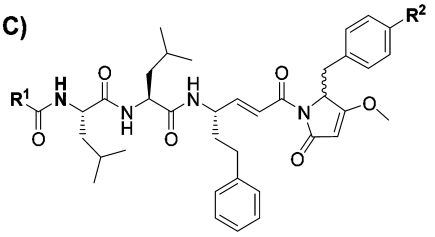

24-33

| Compound | $R^1$ | $R^2$ |
|---|---|---|
| 24 | *N,N*-$Me_2$-L-Val | Ph |
| 25 | 4-(*N*-Me)piperidine | Ph |
| 26 | *N,N*-$Me_2$-L-Val | 4-$CF_3$Ph |
| 27 | 4-(*N*-Me)piperidine | 4-$CF_3$Ph |
| 28 | *N,N*-$Me_2$-L-Val | 4-$OCH_3$Ph |
| 29 | 4-(*N*-Me)piperidine | 4-$OCH_3$Ph |
| 30 | *N,N*-$Me_2$-L-Val | 4-CNPh |
| 31 | 4-(*N*-Me)piperidine | 4-CNPh |
| 32 | *N,N*-$Me_2$-L-Val | Naph |
| 33 | 4-(*N*-Me)piperidine | Naph |

**Figure 3.** Structures of gallinamide A natural product analogues. (A) Gallinamide A **1** and depsipeptide gallinamide A analogues **2**−**10** with variation at the pseudo-*N*-terminus and the $\alpha,\beta$-unsaturated and pyrrolinone units. (B) Indolylpyrrolinone gallinamide A analogues **11**−**23**. (C) Biaryl-functionalized pyrrolinone analogues **24**−**33**.

four independent experiments (Figures S1 and S2). In parallel, 500 SARS-CoV-2 viral particles were used to infect confluent monolayers of A549/ACE2 cells grown in 96-well plates that had been incubated for 1 h with serially diluted gallinamide A, followed by assessment of the formation of CPE 96 h later under an inverted microscope. This showed that gallinamide A, at a concentration as low as 625 nM, was capable of completely preventing virus-induced CPE (Figure S3).

Recent studies have shown that peptidic inhibitors of CatL and other related cysteine proteases also possess inhibitory activity against SARS-CoV-2 Mpro.[40,41] To assess the comparative activity of gallinamide A against human CatL and the viral proteases Mpro and PLpro, we incubated these proteases with 10 $\mu$M of the natural product and quantified the remaining activity using fluorogenic substrates. CatL activity was completely inhibited by gallinamide A at this concentration, while no inhibition of Mpro or PLpro was observed (Figure 1C). Further, we confirmed that gallinamide A also did not inhibit the activity of two other key host proteases facilitating SARS-CoV-2 entry to cells, namely furin and TMPRSS2, up to a concentration of 50 $\mu$M (Figure S4).

We next determined the abundance of CatL in the VeroE6 and A549 cell lines. A comprehensive bottom-up proteomic analysis was utilized to assess the likelihood that this protease serves as the physiological target of gallinamide A in cell-based assays (Figure S5, Data Set S1). In VeroE6 cells, CatL was among the top 300 most abundant proteins, and in comparison, its closely related homologue cathepsin B (CatB) was 10-fold lower in abundance. In contrast, A549 cells had 10-fold higher levels of CatB compared to CatL. In addition to determining the abundance of CatL by proteomics, we confirmed that CatL was catalytically active



https://doi.org/10.1021/acs.jmedchem.1c01494
J. Med. Chem. XXXX, XXX, XXX−XXX

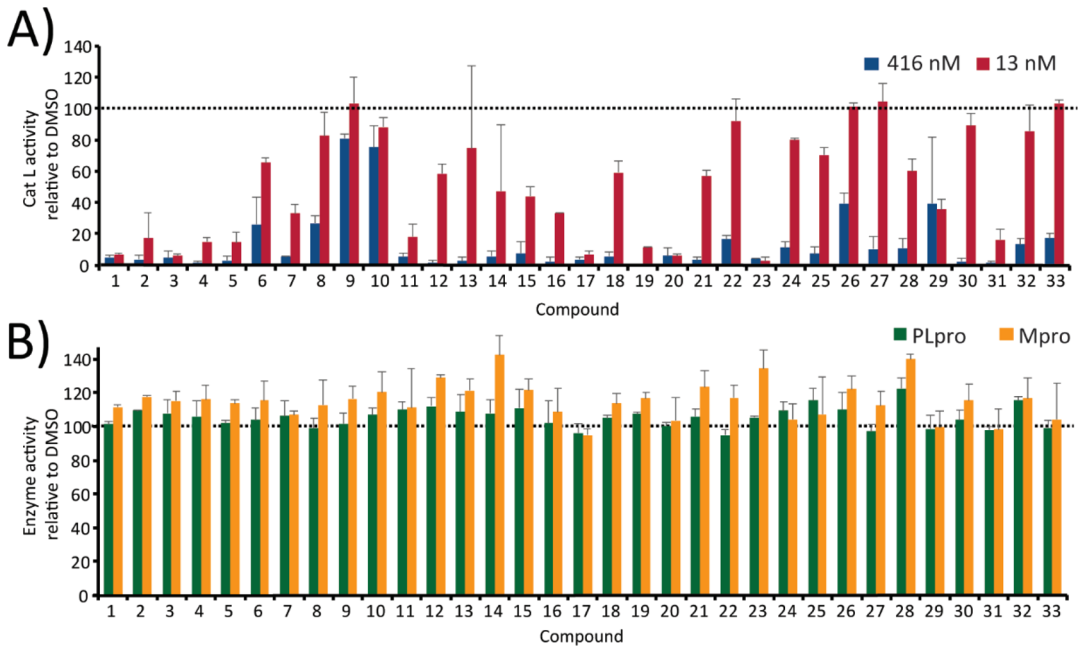


**Figure 4.** Activity of gallinamide A and analogues against cellular and viral proteases. (A) Screening of gallinamide A **1** and analogues **2**−**33** at 13 and 416 nM for inhibition of human CatL. (B) Screening of gallinamide A and analogues at 10 $\mu$M for inhibition against SARS-CoV-2 Mpro and PLpro. Assays were performed in triplicate wells and data are the means ± SD. Activity was compared to reactions containing 0.2% DMSO in assay buffer.

in VeroE6 cells by incubating lysates with the fluorogenic substrate Z-Phe-Arg-AMC. This activity was completely inhibited by 20 $\mu$M of gallinamide A. CatB can also cleave Z-Phe-Arg-AMC, however when a CatB-specific inhibitor, CA-074[42] was added to the lysate, no inhibitory activity was observed (Figure S6A). These data reveal that there is very little active CatB in VeroE6 lysates relative to CatL. For A549 cell extracts, protease activity using Z-Phe-Arg-AMC was also inhibited by gallinamide A, however most of the activity was also sensitive to CA-074 indicating that CatB is the dominant cysteine cathepsin in these cells (Figure S6B). This activity data is supported by our proteomics analysis of A549 cells where CatB was found to be more abundant than CatL (Figure S5). The level of CatL differs substantially in these cell lines which supports published data that some cell lines are more sensitive to cysteine protease inhibition than others.[23]

To further corroborate the protein targets of gallinamide A in cells, VeroE6 cells were treated with a gallinamide A probe molecule bearing an alkyne handle (GalAlkyne) to enable pulldown of targets and identification via proteomics analysis (Figure 2A). We first confirmed that the probe molecule maintained potent inhibitory activity against CatL. The GalAlkyne probe was subsequently incubated with VeroE6 cells, and then biotin azide was reacted with the cell lysate via Cu(I)-catalyzed azide−alkyne cycloaddition. Biotinylated proteins were enriched with streptavidin beads and quantified by proteomics. CatL was the most highly enriched protein in these cells indicating that this enzyme is the primary target of gallinamide A (Figure S7). As expected, CatB, together with other cathepsins, were also enriched but were at least 10-fold lower in abundance than CatL (Figure 2B).

In complementary experiments, VeroE6 cells were treated with native gallinamide A and covalent adducts of GalA-CatL were identified in cell lysates using targeted MS/MS (Figure S8). Adducts were not detectable for other cathepsins, likely due to a combination of the selectivity of gallinamide A for CatL over other cathepsins, and the higher abundance of CatL in VeroE6 cells. Taken together, these data suggest that the antiviral activity of gallinamide A is due to inhibition of host CatL and not due to targeting of the viral proteases (Mpro and PLpro) or other host proteases.

**Assessment of CatL Inhibitory Activity of Synthetic Gallinamide A Analogues.** Three series of synthetic gallinamide A analogues have been developed by our laboratories to date. Series 1 consist of depsipeptide compounds **2**−**10**, with various aliphatic residues incorporated at the pseudo-*N*-terminus, the $\alpha,\beta$-unsaturated moiety and on the pyrrolinone ring (Figure 3).[37] Series 2 is comprised of indolylpyrrolinone analogues **11**−**23** that have varied functionality at the pseudo-*N*-terminus and the three amino acid residues within the linear chain.[39] Finally, series 3 analogues (**24**−**33**) possess a number of biaryl-moieties appended to the pyrrolinone unit, and dimethylvaline or methylpiperidine functionalities at the pseudo-*N*-terminus. Each of these analogues was subjected to a preliminary inhibitory screen against human CatL, Mpro, and PLpro (Figure 4). For the CatL assays, compounds were incubated at 416 nM; the majority of the analogues showed potent inhibition at this concentration, with 21 of the compounds reducing enzymatic activity by more than 90% (Figure 4A). Based on the lack of potency of the parent natural product **1** against Mpro and PLpro, compounds were screened at a higher concentration (10 $\mu$M) against these enzymes. As with gallinamide A, none of these analogues showed appreciable inhibition of SARS-CoV-2 Mpro or PLpro under these conditions (Figure 4B). A follow-up screen against CatL at 13 nM identified gallinamide A (**1**), analogue **3** from series 1, and **17**, **19**, **20**, and **23** from series 2 as being the most potent


https://doi.org/10.1021/acs.jmedchem.1c01494
J. Med. Chem. XXXX, XXX, XXX−XXX

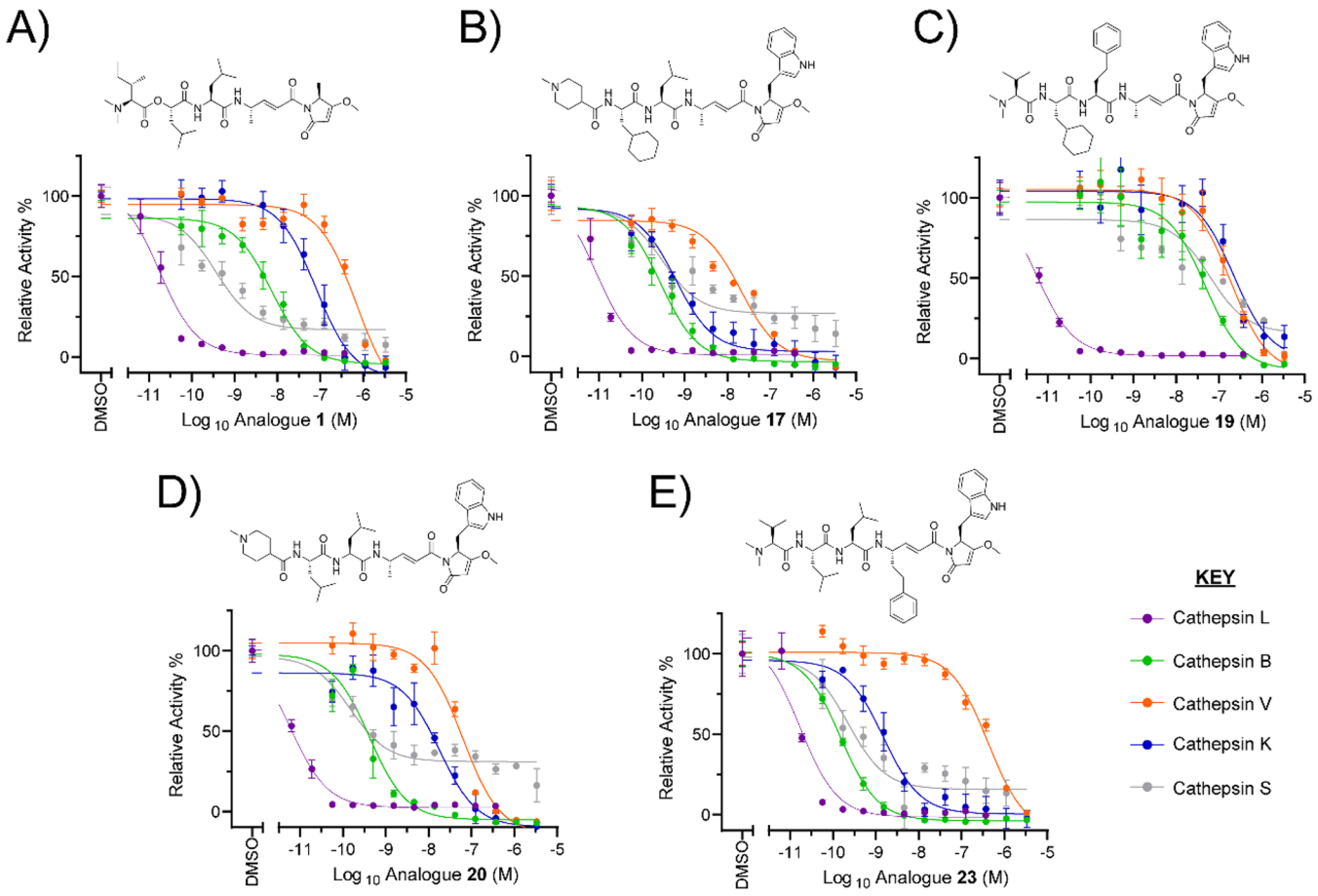


**Figure 5.** Dose−response curves against CatL, CatB, CatV, CatK, and CatS for (A) gallinamide A (**1**) and synthetic analogues (B) **17**, (C) **19**, (D) **20**, and (E) **23**. Activity was normalized to a vehicle control, and all data are the means ± SEM for four technical replicates.

**Table 1. $IC_{50}$ Values of Gallinamide A and Synthetic Analogues against Human Recombinant CatL, CatB, CatV, CatK, and CatS**[a]

| | **1** (μM) | **17** (μM) | **19** (μM) | **20** (μM) | **23** (μM) |
|---|---|---|---|---|---|
| Cat L | $(1.76 \pm 0.32) \times 10^{-5}$ | $(8.57 \pm 1.41) \times 10^{-6}$ | $(5.60 \pm 0.66) \times 10^{-6}$ | $(6.02 \pm 0.66) \times 10^{-6}$ | $(1.70 \pm 0.37) \times 10^{-5}$ |
| Cat B | $(7.34 \pm 1.55) \times 10^{-3}$ | $(2.78 \pm 0.51) \times 10^{-4}$ | $(4.76 \pm 1.78) \times 10^{-2}$ | $(4.16 \pm 0.91) \times 10^{-4}$ | $(1.49 \pm 0.14) \times 10^{-4}$ |
| Cat V | $(6.97 \pm 1.61) \times 10^{-1}$ | $(2.06 \pm 0.45) \times 10^{-2}$ | $(1.86 \pm 0.52) \times 10^{-1}$ | $(6.32 \pm 1.19) \times 10^{-2}$ | $(4.19 \pm 0.82) \times 10^{-1}$ |
| Cat K | $(7.96 \pm 2.03) \times 10^{-2}$ | $(6.23 \pm 1.87) \times 10^{-4}$ | $(2.19 \pm 0.92) \times 10^{-1}$ | $(1.79 \pm 0.487) \times 10^{-2}$ | $(1.50 \pm 0.36) \times 10^{-3}$ |
| Cat S | $(3.67 \pm 1.20) \times 10^{-4}$ | $(3.04 \pm 1.32) \times 10^{-4}$ | $(6.03 \pm 2.58) \times 10^{-2}$ | $(1.49 \pm 0.475) \times 10^{-5}$ | $(2.24 \pm 0.95) \times 10^{-4}$ |
| $EC_{50}$ SARS-CoV-2 | $(2.8 \pm 1.2) \times 10^{-2}$ | $6.07 \pm 2.4$ | $(1.68 \pm 0.67) \times 10^{-1}$ | >5 | $(9.20 \pm 4.3) \times 10^{-1}$ |
| $CC_{50}$ in VeroE6 | >100 | >100 | >100 | >100 | >100 |

[a]Activity was normalized to a vehicle control, and all data are the means ± SD for four technical replicates. $EC_{50}$ values against SARS-CoV-2 infection and $CC_{50}$ in VeroE6 cells. Data are the mean ± SD of 3−4 independent biological replicates (see Figures 5, S2, and S12 for data).

inhibitors. These were selected for more detailed inhibitory assays against human CatL as described below.

The inhibitory potency of gallinamide A (**1**) and analogues **17**, **19**, **20**, and **23** was next evaluated using dose−response assays against CatL for the determination of $IC_{50}$ values (Figure 5 and Table 1). An insufficient amount of analogue **3** was available for these experiments, and therefore no further studies were performed with this compound. Gallinamide A (**1**) exhibited an $IC_{50}$ of 17.6 pM against CatL (Figure 5A), while the four analogues possessed $IC_{50}$ values ranging from 6 to 17 pM (Figure 5B−E). Each of the compounds were counter-screened against related human cysteine cathepsins, including CatB, cathepsin V (CatV), cathepsin K (CatK), and cathepsin S (CatS) (Figure 5A−E). While each of the compounds showed inhibitory activity against all cathepsins tested, the $IC_{50}$ values were generally between 1 and 4 orders of magnitude less potent than for CatL, thus indicating selectivity for CatL over the other cathepsins. In addition to determining the $IC_{50}$ values, we also determined $k_{inact}/K_I^{app}$ values for gallinamide A and the lead analogues for CatL (Table 2, Figure S9). Based on the $k_{inact}/K_I^{app}$, we determined that analogue **23** was 1.4-fold more potent than the parent natural product **1**, while **17**, **19**, and **20** were between 2.1- and 3.2-fold less potent than **1**.

Given that CatB was detected in proteomics studies using VeroE6, A549, MRC5/ACE2/TMPRSS2a, and HEK293/ACE2/TMPRSS2a lysates (Figure S5), and it has also been recently reported that a broad-spectrum activity-based probe for cysteine proteases was active against both proteases in cell lysates,[23] we also calculated the $k_{inact}/K_I^{app}$ values for


https://doi.org/10.1021/acs.jmedchem.1c01494
J. Med. Chem. XXXX, XXX, XXX−XXX

Table 2. $k_{inact}/K_I^{app}$ ($s^{-1}$ $M^{-1}$) Values ± SD for Four Technical Replicates for the Inhibition of Recombinant Human CatL, Human CatB, and Mouse CatL (mCatL) by Gallinamide A (1) and Analogues 17, 19, 20, and 23[a]

| | 1 | 17 | 19 | 20 | 23 |
|---|---|---|---|---|---|
| | | | Cat L | | |
| $k_{inact}$ ($s^{-1}$) | $(4.75 \pm 0.59) \times 10^{-3}$ | $(3.47 \pm 0.19) \times 10^{-3}$ | $(5.87 \pm 0.17) \times 10^{-3}$ | $(8.34 \pm 0.62) \times 10^{-3}$ | $(9.85 \pm 0.57) \times 10^{-3}$ |
| $K_I^{app}$ (M) | $(7.95 \pm 0.32) \times 10^{-9}$ | $(1.80 \pm 0.26) \times 10^{-8}$ | $(3.10 \pm 0.20) \times 10^{-8}$ | $(2.88 \pm 0.48) \times 10^{-8}$ | $(1.18 \pm 0.20) \times 10^{-8}$ |
| $k_{inact}/K_I^{app}$($s^{-1}$ $M^{-1}$) | $5.98 \times 10^5$ | $1.93 \times 10^5$ | $1.89 \times 10^5$ | $2.90 \times 10^5$ | $8.35 \times 10^5$ |
| | | | Cat B | | |
| $k_{inact}$ ($s^{-1}$) | $(6.27 \pm 1.44) \times 10^{-4}$ | $(2.09 \pm 0.32) \times 10^{-2}$ | $(3.35 \pm 0.36) \times 10^{-3}$ | $(1.70 \pm 0.30) \times 10^{-2}$ | $(1.89 \pm 0.66) \times 10^{-3}$ |
| $K_I^{app}$ (M) | $(1.17 \pm 0.77) \times 10^{-7}$ | $(8.61 \pm 1.98) \times 10^{-7}$ | $(3.47 \pm 0.77) \times 10^{-7}$ | $(8.54 \pm 2.26) \times 10^{-7}$ | $(2.38 \pm 1.93) \times 10^{-7}$ |
| $k_{inact}/K_I^{app}$($s^{-1}$ $M^{-1}$) | $5.35 \times 10^3$ | $2.43 \times 10^4$ | $9.65 \times 10^3$ | $1.99 \times 10^4$ | $7.94 \times 10^3$ |
| | | | mCat L | | |
| $k_{inact}$ ($s^{-1}$) | $(5.69 \pm 0.15) \times 10^{-3}$ | $(8.56 \pm 0.96) \times 10^{-3}$ | $(2.24 \pm 0.34) \times 10^{-3}$ | $(3.19 \pm 0.11) \times 10^{-3}$ | $(9.60 \pm 0.32) \times 10^{-3}$ |
| $K_I^{app}$ (M) | $(5.29 \pm 0.48) \times 10^{-9}$ | $(2.93 \pm 0.73) \times 10^{-8}$ | $(1.65 \pm 0.47) \times 10^{-8}$ | $(3.95 \pm 0.42) \times 10^{-9}$ | $(4.15 \pm 0.51) \times 10^{-9}$ |
| $k_{inact}/K_I^{app}$($s^{-1}$ $M^{-1}$) | $1.07 \times 10^6$ | $2.92 \times 10^5$ | $1.36 \times 10^5$ | $8.06 \times 10^5$ | $2.31 \times 10^6$ |

[a]See Figures S9–S11 for data.

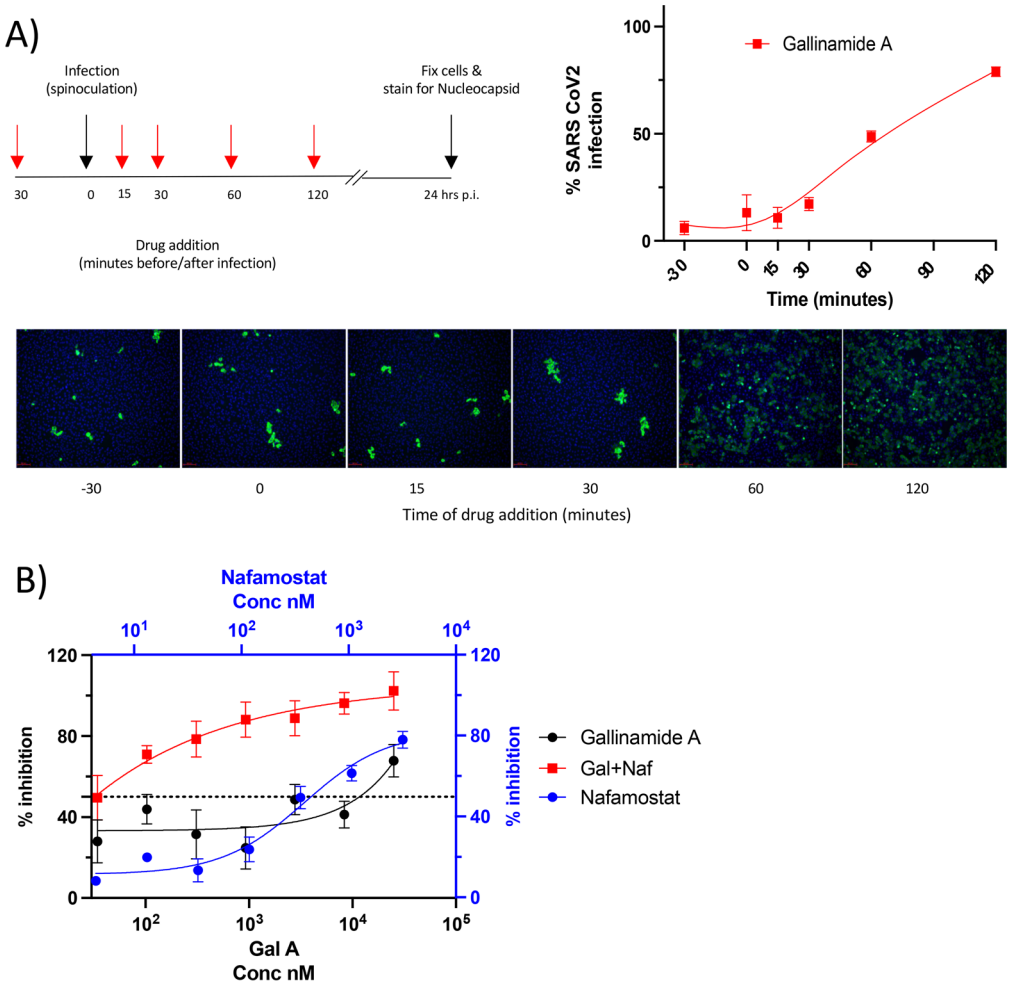


Figure 6. Gallinamide A (1) inhibits viral entry into VeroE6 cells and synergizes with TMPRSS2-inhibition to increase anti-SARS-CoV-2 efficacy. (A) Time of addition study to establish the kinetics of gallinamide A inhibitory activity on SARS-CoV-2 infection. Gallinamide A (0.5 μM) was added at the times indicated prior to or after infection (spinoculation) of VeroE6 cells. At 24 h postinfection, cells were stained with antinucleocapsid antibody (green) and Hoechst dye (blue) to determine the percentage of infected cells. Representative images for the various test conditions are shown, scale bar 100 μm. (B) Inhibition of SARS-CoV-2 infection by gallinamide A (1), in comparison to and in synergism with the TMPRSS2 protease inhibitor nafamostat mesylate, directly compared in ACE2/TMPRSS2 expressing HEK293 cells. Data are the means ± SD and are representative of three independent replicates.

gallinamide A and the selected lead analogues against CatB. This revealed selectivity values ranging from 8-fold for compound 17 to 112-fold for gallinamide A (1) (Table 2, Figure S10) for CatL over CatB. In addition, we evaluated the molecules against mouse CatL (mCatL) to give an initial indication of the future applicability in mouse models of


https://doi.org/10.1021/acs.jmedchem.1c01494
J. Med. Chem. XXXX, XXX, XXX−XXX

SARS-CoV-2 infection. With the exception of **19**, the compounds possessed increased potency against mCatL relative to human CatL (Table 2, Figure S11).

**Inhibition of SARS-CoV-2 Entry into Cells.** To provide further evidence that the antiviral activity of gallinamide A was due to inhibition of CatL-mediated endosomal entry, we performed time of addition studies in VeroE6 cells. To synchronize virus entry, SARS-CoV-2 was spinoculated onto cells, then incubated at 37 °C. Gallinamide A (**1**) was added at various time points to the cell culture, from 30 min preinfection to 120 min postinfection. At 24 h postinfection, cells were fixed and stained with antinucleocapsid antibody to enumerate cells positive for virus. The inhibitory effect was maximum when **1** was added prior to or at the time of entry, with efficacy reducing substantially when added at 60 min or later postinfection, consistent with the kinetics of inhibition of endosomal entry (Figure 6A).

Having established the potent inhibition of CatL and SARS-CoV-2 entry by gallinamide A, and having also demonstrated that synthetic analogues **17**, **19**, **20**, and **23** were also potent inhibitors of the protease, we next assessed these lead analogues against SARS-CoV-2 entry and infectivity in VeroE6 cells. Before embarking on the antiviral assays, each of the analogues were first assessed for cytotoxicity on VeroE6 cells. Pleasingly, none of the compounds exhibited notable cytotoxicity after 72 h at concentrations up to 100 $\mu$M in this cell line (Figure S12). Antiviral assays were next performed in VeroE6 cells on the lead analogues using the same high content fluorescence microscopy method described for gallinamide A above. Analogues **19** and **23** both exhibited potent antiviral activity with $EC_{50}$ values of 168 nM and 920 nM, respectively (Table 1, Figure S2). Based on these data, we further assessed the activity of the compounds against SARS-CoV-2-induced CPE in A549/ACE2 cells. In these experiments, complete inhibition of CPE was observed at concentrations of 310 nM for **19** and **23** (Figure S3), making them more potent than gallinamide A in these cells. Interestingly, in both cell lines, **17** and **20** exhibited poor antiviral activity with $EC_{50}$ values greater than 5 $\mu$M, despite showing potent inhibition of CatL *in vitro* ($IC_{50}$ of 9 and 6 pM, respectively) and complete inactivation of CatL in VeroE6 and A549 lysates at 10 $\mu$M (Figure S6). The reduced activity of **17** and **20** compared to **1**, **19** and **23** in the antiviral assay may be owing to poor cell permeability of these compounds.

**Efficacy of CatL Inhibition in TMPRSS2 Positive Cells and Synergism with a TMPRSS2 Inhibitor.** While both CatL and TMPRSS2 can mediate SARS-CoV-2 entry into target cells by facilitating S protein priming,[22] the predominant mechanism of entry is dependent on the relative levels of the two proteins in a given cell line.[19,28,41] Therefore, to assess the effect of the lead compounds **1** and **19** in a TMPRSS2 overexpressing cell line, we used MRC-5/ACE2/TMPRSS2 cells which we also verified to possess CatL, albeit in lower abundance than in VeroE6 and A549 cells (Figure S5). Gratifyingly, both **1** and **19** were able to completely neutralize SARS-CoV-2 entry into this cell line at a concentration of 32 nM (Figure S13), thus suggesting that CatL is still important for viral entry in these TMPRSS2 overexpressing cells. Interestingly, while the TMPRSS2 inhibitor Nafamostat mesylate was able to block infection in MRC-5/ACE2/TMPRSS2 (albeit with neutralization at 4 $\mu$M concentrations), it did not exhibit notable antiviral activity on VeroE6 cells (Figure S13). These data suggest that both TMPRSS2 and CatL protease pathways are operational and important for infectivity in MRC-5/ACE2/TMPRSS2 cells, but that CatL is the predominate pathway in VeroE6 cells, consistent with the levels of each protein in these cells (Figure S5).

We also assessed the activity of gallinamide A (**1**) in another TMPRSS2 overexpressing cell line, HEK293-ACE2-TMPRSS2, which express CatL but at an even more substantially reduced abundance compared to VeroE6, and also reduced compared to MRC5 cells (Figure S5). Here, in the context of TMPRSS2 overexpression, the antiviral activity of gallinamide A was substantially reduced compared to that observed in VeroE6 cells, where endosomal entry of the virus predominates. In contrast, the TMPRSS2 inhibitor nafamostat mesylate possessed potent antiviral activity in the HEK293-ACE2-TMPRSS2 (Figure 6B) cells but was not effective in the VeroE6 line (Figure S13). Of interest, combined use of gallinamide A with nafamostat mesylate in HEK-ACE2-TMPRSS2 cells showed synergistic antiviral activity (Figure 6B, Figure S14). This suggests that endosomal entry inhibitors, like gallinamide A, may find use as therapeutics when used in combination with inhibitors of other pathways of viral entry, such as TMPRSS2.

## DISCUSSION AND CONCLUSIONS

Pathogenic coronaviruses are now well-recognized for their potential to induce substantial human morbidity and mortality. To bring the current global pandemic of SARS-CoV-2 under control will ultimately require mass implementation of safe and effective vaccines. While recent vaccine results have been very promising, the rise in breakthrough infections in fully vaccinated individuals is a concern, and highlights the importance of having alternative strategies to manage the pandemic and protect unvaccinated individuals or vulnerable populations. In previous epidemics, where vaccines were limited, either by efficacy or reach within the community, antivirals served as the cornerstone for fighting disease. This has been recently observed for two major viral pathogens, HCV, which is now readily curable with a short course of antivirals, and HIV. While HIV cannot be cured by therapeutic approaches, it can be readily managed through pre-exposure prophylaxis (PreP) or treatment postexposure with antivirals. While it is acknowledged that respiratory diseases like SARS-CoV-2 present many unique challenges with respect to antiviral strategies, it is feasible that equivalent success in PreP development could in turn lead to the protection of vulnerable communities, such as healthcare workers or the elderly within care facilities. In addition, PreP-based approaches may reduce the viral reproductive rate in communities with high SARS-CoV-2 prevalence. Even if PreP antiviral strategies were limited to lowering viral load, this would improve not only prognosis but also limit the onward spread to the next host.

Early in pandemics, clinically ready drugs provide the fastest means for effective treatment. To date, many repurposed drugs have not provided any evidence of clinical benefit for SARS-CoV-2, except for dexamethasone for late-stage disease. However, dexamethasone is a steroid rather than an antiviral agent. With the virus entrenched within the global population and new more infectious strains emerging,[43] we now require compounds that target the virus with greater potency and breadth. Previous studies have indicated that CatL inhibitors


https://doi.org/10.1021/acs.jmedchem.1c01494
J. Med. Chem. XXXX, XXX, XXX−XXX

have the potential to serve as antivirals for a range of coronaviruses, including HCoV-229E,[44] MERS-CoV,[45] and SARS-CoV-1.[46] SARS-CoV-2 spike-mediated cell entry is enhanced by overexpression of CatL in human cell lines, and recent evidence suggests elevated levels of circulating CatL is also correlated with COVID-19 disease progression and severity.[24] CatL is also one the most highly upregulated proteins in the lungs of deceased individuals with COVID-19 disease, which suggests that CatL activity may also drive inflammation.[47] Importantly, targeting a host protease, as opposed to a viral protease specific to one virus or viral strain, may provide the best opportunity for broad spectrum antiviral activity that is less susceptible to rapidly progressing viral mutations. CatL is therefore a promising drug target for SARS-CoV-2, for other current or future coronavirus strains, as well as other virus families, including the *Filoviridae*, such as the Ebola virus.[45]

Historically, nature has been the single most successful source for the discovery of new pharmaceutical lead compounds, especially in the areas of anti-infective and anticancer agents.[48,49] In this work, we demonstrate that gallinamide A, a peptide-based natural product isolated from a Panamanian marine cyanobacterium, and two synthetic analogues of the natural product, possess potent activity against SARS-CoV-2 infectivity in monkey (VeroE6) and human (A549) cells. Specifically, the parent natural product exhibited the most potent inhibition of SARS-CoV-2 in VeroE6 cells, with an $EC_{50}$ of 28 nM, whereas analogues **19** and **23** were the most potent in A549/ACE2 cells (complete inhibition of CPE at 310 nM). We show that these molecules were able to inhibit CatL in both cell lines, and could selectively target recombinant CatL over other related cysteine cathepsins *in vitro*, with no VeroE6 cell cytotoxicity at 72 h up to 100 $\mu$M. Based on this potent CatL inhibitory activity of gallinamide A, and the structural analogues, it is tempting to speculate that the evolution of this cyanobacterially derived molecule has been guided and optimized by activity at a cysteine protease target related to CatL.

CatL is a lysosomal enzyme that plays a key role in intracellular protein degradation in our cells. Expression of this enzyme is dysregulated in several human diseases, including cancer,[50] arthritis,[51] and diabetic nephropathy,[52] with therapeutics in development for these ailments.[53] Mice deficient for this gene exhibit hair loss,[54] bone and heart defects,[55,56] and enhanced susceptibility to bacterial infection.[57] Therefore, targeting of this host enzyme for treatment of SARS-CoV-2 infections may pose a risk for side-effects. However, treatment for coronavirus infection would likely be short-term, aiming to reduce viral entry and early replication until host innate and adaptive responses can be developed. There are already a number of FDA-approved drugs that possess inhibitory activity against CatL.[27] Furthermore, recent studies have shown that K777, a potent irreversible inhibitor of CatL consisting of a dipeptide-vinyl sulfone, was found to be well-tolerated in rodents, dogs, and nonhuman primates,[58] and an investigational new drug application (IND) has been opened with the FDA for its use as a therapeutic treatment of COVID-19 infection.[23] Importantly, synthetic gallinamide A analogues have already been examined *in vivo* for other infectious indications.[39] Our studies showed that gallinamide A and the most promising synthetic analogues maintain potency against mouse CatL.

While CatL shows clear promise as a suitable drug target, the entry pathways for SARS-CoV-2 are complex and can be endosomal or at the cell membrane, with the latter driven by the serine protease TMPRSS2.[19] When cellular expression of TMPRSS2 is high, this is the preferential route of viral entry; however, with reduced TMPRSS2, SARS-CoV-2 will utilize the endosomal entry pathway involving CatL, a phenomenon that may in part explain the inefficacy of hydroxychloroquine as a therapeutic.[59,60] Indeed, in our study, TMPRSS2 inhibition provided superior antiviral activity compared to CatL inhibition in cells overexpressing TMPRSS2, but when both viral entry pathways were targeted, this resulted in a synergistic potentiation of the antiviral activity (Figure 6B). Tropism of the virus *in vivo* is equally complex. Oropharyngeal tissue is well-known for its ability to facilitate transmission and contributes to the early stages of disease, while once established, infection can proceed across many organ types outside of the respiratory tract, including kidneys, liver, heart, brain, and blood.[61] CatL and TMPRSS2 are both highly expressed in lung tissue;[62] however, treatment of infection across multiple different cell types and organ systems may require preferential inhibition at the membrane (TMPRSS2) or in the endosome (CatL). Future studies will therefore seek to further investigate incorporation of inhibitors of the major fusogenic entry pathways for the virus. This combination approach may have an added benefit in that it may allow lower doses of the individual drugs to be utilized due to synergism in their mechanism of action. Additionally, it may be that no compound will provide adequate therapeutic efficacy long-term when used as monotherapy, as this will likely drive drug resistance, as has been seen for HIV and hepatitis. Combination drug regimens would be highly preferable, including drugs that target host proteases, which are less likely to be substantially impacted by the emergence of viral variants.

In summary, we demonstrate here that the marine natural product, gallinamide A, and several synthetic analogues, are potent inhibitors of CatL, a key host cysteine protease involved in the pathogenesis of SARS-CoV-2. Lead molecules possessed selectivity over CatB and other related human cathepsins or proteases used for SARS-CoV-2 entry and did not exhibit inhibitory activity against viral proteases Mpro and PLpro. Gallinamide A and two lead analogues potently inhibited SARS-CoV-2 infection *in vitro* and, importantly, gallinamide A also exhibited synergism in antiviral activity when used in combination with a TMPRSS2 inhibitor. This work therefore highlights the potential of CatL as a bona fide target for the development of novel antivirals for SARS-CoV-2 or other pathogenic coronaviruses.

## EXPERIMENTAL SECTION

**General Synthetic Chemistry Methods.** The synthesis of gallinamide A analogues **2**–**10** and **11**–**23** was carried out as previously reported by Boudreau et al.[37] and Stoye et al.,[39] respectively. The isolation of the natural product gallinamide A was carried out as previously reported by Linington et al.[33] General synthetic materials and methods and full synthetic details and characterization of analogues **24**–**33** and GalAlkyne (based on the method from Stoye et al.[39]) are described in the Supporting Information. All final compounds were >95% pure by HPLC analysis.

**Protease Screening of Gallinamide A (1) and Analogues 2**–**33.** Recombinant SARS-CoV-2 Mpro was expressed and purified as described previously.[23] This enzyme (200 nM) was incubated with 10 $\mu$M of each compound at 25 °C in 20 mM Tris-HCl pH 7.5, 150


https://doi.org/10.1021/acs.jmedchem.1c01494
J. Med. Chem. XXXX, XXX, XXX−XXX

mM NaCl, 1 mM DTT, 5% glycerol, 0.01% Tween-20 for 15 min. An equal volume of 200 $\mu$M Mu-HSSKLQ-AMC (Sigma-Aldrich, SCP0224) in the same buffer was then added, and protease activity was quantified at 25 °C. Recombinant SARS-CoV-2 PLpro was purchased from Acro Biosystems, PAE-C5184. 49 nM of this enzyme was incubated with 10 $\mu$M of each compound at 25 °C for 15 min in 50 mM HEPES, 150 mM NaCl, 1 mM DTT, 0.01% Tween 20; pH 6.5. An equal volume of 50 $\mu$M Z-RLRGG-AMC (Bachem, I1690) in the same buffer was then added to start the reaction. Recombinant human Cathepsin L was purchased from R&D Systems (952-CY), and 50 pM of the enzyme was incubated with 416 nM and 13 nM of each compound and separately with 10 $\mu$M of gallinamide A at 25 °C for 15 min in 50 mM sodium acetate pH 5.5, 5 mM DTT, 0.01% BSA, 1 mM EDTA. An equal volume of 5 $\mu$M of Z-FR-AMC (Sigma-Aldrich, C9521) was then added. Recombinant human TMPRSS2 was purchased from Cusabio Technology (CSB-YP023924HU) and assayed with 86 $\mu$M Boc-QAR-AMC in 25 mM Tris-HCl, 150 mM NaCl, 5 mM $CaCl_2$, 0.01% Triton X-100, pH 8.0 at a final concentration of 3 nM. Recombinant human furin was purchased from R&D Systems (1503-SE) and assayed in 25 mM Tris-HCl, 150 mM NaCl, 5 mM $CaCl_2$, 0.01% Triton X-100, pH 8.0 with 50 $\mu$M pERTKR-AMC at a final concentration of 1.9 nM. TMPRSS2 and furin were preincubated with 100 $\mu$M of Gallinamide A and analogs for 30 min prior to addition of substrate. All assays were performed at room temperature in triplicate wells and DMSO was used as a vehicle control. The final volume of each reaction was 30 $\mu$L, and fluorescence was measured at 360/460 nm (ex/em) using a Biotek Synergy M2 fluorescence plate reader. Activity was normalized to wells lacking inhibitor but containing 0.01% DMSO in assay buffer.

**Dose−Response Studies.** Recombinant human cathepsin B (953-CY), cathepsin S (1183-CY), and cathepsin V (1080-CY) were purchased from R&D Systems. Human cathepsin K (BML-SE553) was purchased from Enzo, and 1.11 nM cathepsin L, cathepsin B, cathepsin V, and cathepsin K and 4.44 nM cathepsin S were preincubated for 30 min at 25 °C with 3333 to 0.006 nM of each compound in 40 mM sodium acetate pH 5.5, 5 mM DTT, 0.001% BSA, 1 mM EDTA, 100 mM NaCl. Remaining protease activity was then detected using a final concentration of 40 $\mu$M of Z-FR-AMC (Sigma-Aldrich, C9521). Fluorescent activity was recorded as outlined above. For $k_{inact}/K_I^{app}$ studies, mouse cathepsin L (1515-CY) was purchased from R&D Systems. Human CatL, human CatB, and mouse CatL (1 nM) were assayed at 25 °C in 30 $\mu$L reaction volumes containing 40 mM sodium acetate pH 5.5, 5 mM DTT, 0.001% BSA, 1 mM EDTA, 100 mM NaCl, 40 $\mu$M of Z-FR-AMC (Sigma-Aldrich, C9521) in the presence of 555.56 to 0.01 nM of each compound in quadruplicate wells. To calculate the $IC_{50}$, inhibitor and substrate were added simultaneously to the enzyme, and the rate of AMC release was determined from 0 to 30 min and compared to a DMSO control. To calculate $K_I^{app}$ and $k_{inact}$, the rate of product formation was calculated at 6 min intervals for 1 h and normalized to activity in the control wells containing DMSO using the equation $k_{obs} = k_{inact}[I]/(K_I^{app} + [I])$. $k_{obs}$ values for each inhibitor concentration were calculated from inactivation curves, and inhibition constants $k_{inact}$ and $K_I^{app}$ were calculated by nonlinear regression of $k_{obs}$ and inhibitor concentration using GraphPad Prism 9 software and the ratio of $k_{inact}/K_I^{app}$ was calculated to assess potency of the inhibitor.[63]

**Cytotoxicity Assays.** Cytotoxicity of lead compounds was determined by an Alamar Blue HS (Invitrogen) cell viability assay as per manufacturer's instructions. Briefly, VeroE6 (ATCC CRL-1586) cells were grown in Dulbecco's Modified Eagle Medium (DMEM) with 4.5 g/L D-Glucose, L-Glutamine and 110 mg/L sodium pyruvate (Gibco), 10% fetal calf serum (Sigma) and penicillin-streptomycin (100 U/ml, Gibco). Five $\times 10^4$ cells were seeded into wells of a 96-well flat bottom culture plate (Corning) and once adhered, compounds were added at varying concentrations and incubated for 24 or 72 h (37 °C, 5% $CO_2$). Alamar Blue HS cell viability reagent (Invitrogen) was added, and the cells further incubated for 2−4 h. Relative fluorescent units (RFU) were determined per well at ex/em 560/590 nm (Tecan Infinite M1000 pro plate reader). Increasing RFU is proportional to cell viability.

**Cell Lines for SARS-CoV-2 Infection Assays.** VeroE6 cells (ATCC CRL-1586) were maintained in Minimal Essential Media (Invitrogen) supplemented with 10% FBS and subcultured according to the supplier's instructions. MRC-5 cells (ATCC CCL-171) and HEK293T cells stably expressing human ACE2 and TMPRSS2 were generated by transducing cells with lentiviral particles. Briefly, the ORFs for hACE2 (Addgene#1786) and hTMPRSS2a (Addgene#53887, synthetic gene fragment; IDT) were cloned into lentiviral expression vectors pRRLsinPPT.CMV.GFP.WPRE[64] and pLVX-IRES-ZsGreen (Clontech), respectively. Lentiviral particles expressing the above proteins were produced by cotransfecting expression plasmids individually with a second generation lentiviral packaging construct psPAX2 (courtesy of Dr Didier Trono through NIH AIDS repository) and VSVG plasmid pMD2.G (Addgene#2259) in HEK293T cells (Life Technologies) by using polyethylenimine as previously described.[65] Two successive rounds of lentiviral transductions were then performed on MRC-5 and HEK293T cells to generate MRC-5/ACE2/TMPRSS2a and HEK293/ACE2/TMPRSS2a cells, respectively. For HEK293/ACE2/TMPRSS2a cells, clonal selection led to the identification of a highly permissive clone, HekAT24, which was then used to carry out SARS-CoV-2 inhibition assay.[66] Human A549 cells stably transduced with human ACE2 viral receptor (A549/ACE2) were grown in M-10 medium.

**Detection of Gallinamide A Protein Targets from VeroE6 Cells.** VeroE6 cells (80−90% confluent) in 6-well plates were treated with gallinamide A **1** only, or gallinamide A-alkyne probe (GalAlkyne), at 10 $\mu$M for 1 h (performed in triplicate). The cells were washed 3 times with DPBS, lysed in 4% SDS buffer (4% SDS, 150 mM NaCl, 50 mM HEPES pH 7.4) containing cOmplete ULTRA Mini, EDTA-free protease inhibitor cocktail (Roche, Sigma), and immediately heated to 95 °C for 10 min. Protein quantitation (Bradford, Sigma) was performed on the lysates, and 1 mg protein was used for a Cu(I)-catalyzed click reaction (CuAAC) to azide-derived biotin and protein precipitated.[67] The protein pellet was resuspended in 4% SDS buffer and then incubated with streptavidin magnetic beads (Pierce) to enrich for biotinylated targets. After binding, beads were washed 6× with 1% SDS in PBS then 4× with PBS. Bound protein was eluted by heating to 95 °C for 10 min in 4% SDC buffer (4% sodium deoxycholate, 0.1 M Tris-HCl pH 8.0). To identify gallinamide A-CatL covalent adducts in cells, VeroE6 cells were treated with gallinamide A as above and then lysed in 4% SDC buffer before proceeding to proteomics analysis.

**Proteomics and Activity Assays Using Cell Lysates.** For proteomics, cell lysates, or eluates from streptavidin-bead enrichment, were digested to peptides and purified using a protocol described previously.[68] Peptide mixtures were analyzed by nanoflow LC-MS/MS as described. Identification and label-free quantification were performed using either MaxQuant, or Byonic (Protein Metrics), with a 1% false discovery rate at both the peptide and the protein level using a target-decoy approach. The HEK293, MRC5, and A549 cells were analyzed using the *Homo sapiens* proteome database and the VeroE6 cells using the *Chlorocebus sabaeus* proteome database, both of which were downloaded from Uniprot. The identification of the gallinamide A covalent adduct on cathepsin L was performed using a wildcard search for potential adducts on cysteine ranging from −40 to 600 Da. This adduct was quantified in VeroE6 cell lysates using a targeted parallel reaction monitoring acquisition method. Isolation of precursor ions at $m/z$ 807.3928 (+4) NQGQC(Cam)GSC(GalA)-WAFSATGALEGQMFRK, and $m/z$ 1033.4898 (+3) NQGQC-(GalA)GSC(Cam)WAFSATGALEGQMFR with a window of 0.7 Th, prior to HCD fragmentation and orbitrap spectral acquisition was performed on a Thermo Eclipse Orbitrap mass spectrometer. All the raw MS data and corresponding search outputs have been deposited to the ProteomeXchange Consortium (http://proteomecentral.proteomexchange.org) via the PRIDE partner repository with the data set identifier PXD027300.


https://doi.org/10.1021/acs.jmedchem.1c01494
J. Med. Chem. XXXX, XXX, XXX−XXX

For activity assays, VeroE6 and A549 cells were lysed by sonication in 50 mM MES pH 6.0; 100 μM AEBSF, 1 μM pepstatin A, 1 mM EDTA, 1 mM DTT buffer and protein concentration in the cleared supernatant was quantified using the bicinchoninic acid assay with BSA as a protein standard. 225 ng of total protein was incubated with 20 μM of **1**, **17**, **19**, **20**, **23**, CA-074 (MilliporeSigma #205530), and E-64 (Alfa Aesar #J62933) for 30 min in 50 mM sodium acetate pH 5.5; 5 mM DTT; 1 mM EDTA; 1 μM pepstatin; 100 μM AEBSF, and then mixed with equal volume of 50 μM of Z-Phe-Arg-AMC in the same buffer. Activity was normalized to wells that lacked inhibitor but contained 0.2% DMSO in assay buffer.

**SARS-CoV-2 Virus Inhibition *in Vitro* Assays.** A high content fluorescence microscopy approach was used to assess the ability of gallinamide A and the synthetic analogues to inhibit SARS-CoV-2 infection in permissive cells. The compounds were initially diluted in cell culture medium (MEM-2% FCS or DMEM-5% FCS) to make 2× working stock solutions and then serially diluted further in the above media to achieve a 2-fold dilution series. For Vero-E6 cells, 20 μL of each dilution was then added to cells seeded a day prior at $3 \times 10^3$ cells in a volume of 40 μL of MEM-2% FCS per well in a 384-well plate (Corning #CLS3985). The plates containing the cells and compounds were incubated for 30 min at 37 °C, 5% $CO_2$ following which 20 μL of virus solution at $8 \times 10^3$ TCID50/mL[69] was added to the wells. Plates were incubated at 37 °C, 5% $CO_2$ for a further 72 h, following which the cells were stained with NucBlue dye (Invitrogen, #R37605) according to manufacturer's instructions. For assays carried out with HekAT24, cells were trypsinized, stained with Nucblue in suspension and then seeded at 16,000 cells in a volume of 40 μL of DMEM-5% FCS per well in a 384-well plate. The cells and antagonists were incubated as described above before adding the virus solution. Plates were incubated at 37 °C, 5% $CO_2$ for a further 24 h. Stained cells were then imaged using the InCell 2500 (Cytiva) high throughput microscope, with a 10× 0.45 NA CFI Plan Apo Lambda air objective. Acquired nuclei were then counted in high content using InCarta high-content image analysis software (Cytiva) to give a quantitative measure of CPE. Virus inhibition/neutralization was calculated as $\%N = (D - (1 - Q)) \times 100/D$, where "$Q$" is the value of nuclei in test well divided by the average number of nuclei in untreated uninfected controls, and "$D$" = 1 − Q for the wells infected with virus but untreated with inhibitors. Thus, the average nuclear counts for the infected and uninfected cell controls get defined as 0% and 100% neutralization, respectively. To account for cell death due to drug toxicity, cells treated with a given compound alone and without virus were included in each assay. The percent neutralization for each compound concentration in infected wells was normalized to percent neutralization in wells with equivalent amount of compound but without the virus to yield the final neutralization values for each condition. Inhibition curves and 50% ($EC_{50}$) effective concentrations were determined by nonlinear regression analysis using GraphPad Prism software (version 9.1.2, GraphPad software, United States).

Time of addition experiments were performed as described previously to determine kinetics of gallinamide A inhibitory activity on SARS-CoV-2 infection.[70] Briefly, VeroE6 cells were seeded at a density of 30 000 cells per well in 100 μL cell culture media following which gallinamide A (0.5 μM) was added at various times prior to or after infection with SARS-CoV-2 (MOI of 0.05). To synchronize infection, virus was spinoculated onto cells at 1200*g* for 40 min at 4 °C. At 24 h post infection, cells were fixed and stained for nucleocapsid as previously described.[65] Briefly, cells were fixed in 4% paraformaldehyde (Electron Microscopy Sciences) and then neutralized with 50 mM $NH_4Cl$ (Sigma) for 3 min. Cells were permeabilized with 0.05% Triton-X (Sigma) for 1 min at room temperature, stained with mouse monoclonal antinucleoprotein antibody (Cell Biolabs, Australia) at 5 $\mu g \cdot ml^{-1}$ followed by rabbit antimouse Alexa Fluor 488 (IgG H+L; highly cross absorbed, Invitrogen). Cells were then counterstained with Hoechst dye (NucBlue, Invitrogen) before imaging using InCell 2500 high throughput microscope, with a 10× 0.45 NA CFI Plan Apo Lambda air objective. Cells positive for Nucleocapsid were enumerated using InCarta and normalized to total cell numbers to calculate percentage of infected cells.

To assess the combined effect of gallinamide A and nafamostat mesylate on SARS-CoV-2 infection the constant-ratio drug combination method was followed.[71,72] Briefly, the inhibitors were mixed in a constant ratio of their respective $EC_{50}$s (molar ratio of 7:1) and a 3-fold dilution series was done with several concentration points above and below the $EC_{50}$ value. Combinations thus generated were tested for their ability to inhibit virus infection in HekAT24 cells as described above. The effect of combination on SARS-CoV-2 infection was examined using median effect principle to calculate combination index values (Calcusyn software package, Biosoft, Cambridge, UK).[73,74] All experiments using infectious virus were conducted under PC3 conditions.

At the University of Texas Medical Branch, A549/ACE2 cells were grown in M-10 media and treated with 500 SARS-CoV-2 viral particles (USA_WA1/2020 isolate) prior to addition of 20 to 0.156 μM of compound. After cultivation at 37 °C for 4 days, individual wells were observed by an inverted microscope for determining the status of virus-induced formation of cytopathic effect (CPE). The efficacy of individual compounds was calculated and expressed as the lowest concentration capable of completely preventing virus-induced CPE in 100% of the wells. All compounds were dissolved in 100% DMSO as 10 mM stock solutions and diluted in culture media. All experiments using infectious virus were conducted under BSL-3 conditions.

## ■ ASSOCIATED CONTENT

### Supporting Information

The Supporting Information is available free of charge at https://pubs.acs.org/doi/10.1021/acs.jmedchem.1c01494.

Supplementary Figures S1−S14 and methods, including general chemical synthesis of analogues, analytical HPLC traces, and NMR spectra for compounds **24**−**33** (PDF)

Raw proteomics data of cell lines utilized (XLSX)

Molecular formula strings (SMILES) for compounds **1**−**33** (CSV)

## ■ AUTHOR INFORMATION


### Corresponding Authors

**William H. Gerwick** − *Skaggs School of Pharmacy and Pharmaceutical Sciences, University of California, San Diego, La Jolla, California 92093, United States; Center for Marine Biotechnology and Biomedicine, Scripps Institution of Oceanography, University of California San Diego, La Jolla, California 92093, United States*; Email: wgerwick@health.ucsd.edu

**Anthony J. O'Donoghue** − *Skaggs School of Pharmacy and Pharmaceutical Sciences, University of California, San Diego, La Jolla, California 92093, United States*; Email: ajodonoghue@health.ucsd.edu

**Richard J. Payne** − *School of Chemistry, The University of Sydney, Sydney, NSW 2006, Australia; Australian Research Council Centre of Excellence for Innovations in Peptide and Protein Science, The University of Sydney, Sydney, NSW 2006, Australia*; orcid.org/0000-0002-3618-9226; Email: richard.payne@sydney.edu.au

### Authors

**Anneliese S. Ashhurst** − *School of Chemistry, The University of Sydney, Sydney, NSW 2006, Australia; School of Medical Sciences, Faculty of Medicine and Health, The University of Sydney, Sydney, NSW 2006, Australia*




https://doi.org/10.1021/acs.jmedchem.1c01494
J. Med. Chem. XXXX, XXX, XXX−XXX

**Arthur H. Tang** − *School of Chemistry, The University of Sydney, Sydney, NSW 2006, Australia*
**Pavla Fajtová** − *Skaggs School of Pharmacy and Pharmaceutical Sciences, University of California, San Diego, La Jolla, California 92093, United States; Institute of Organic Chemistry and Biochemistry, Academy of Sciences of the Czech Republic, 16610 Prague, Czech Republic*
**Michael C. Yoon** − *Skaggs School of Pharmacy and Pharmaceutical Sciences, University of California, San Diego, La Jolla, California 92093, United States;* orcid.org/0000-0002-2900-5257
**Anupriya Aggarwal** − *Kirby Institute, University of New South Wales, Sydney, NSW 2052, Australia*
**Max J. Bedding** − *School of Chemistry, The University of Sydney, Sydney, NSW 2006, Australia*
**Alexander Stoye** − *School of Chemistry, The University of Sydney, Sydney, NSW 2006, Australia*
**Laura Beretta** − *Skaggs School of Pharmacy and Pharmaceutical Sciences, University of California, San Diego, La Jolla, California 92093, United States*
**Dustin Pwee** − *Skaggs School of Pharmacy and Pharmaceutical Sciences, University of California, San Diego, La Jolla, California 92093, United States*
**Aleksandra Drelich** − *Department of Microbiology and Immunology, University of Texas, Medical Branch, Galveston, Texas 77755-1001, United States*
**Danielle Skinner** − *Skaggs School of Pharmacy and Pharmaceutical Sciences, University of California, San Diego, La Jolla, California 92093, United States*
**Linfeng Li** − *Department of Biochemistry and Biophysics, Texas A&M University, College Station, Texas 77843, United States;* orcid.org/0000-0001-6185-4999
**Thomas D. Meek** − *Department of Biochemistry and Biophysics, Texas A&M University, College Station, Texas 77843, United States;* orcid.org/0000-0002-1931-8073
**James H. McKerrow** − *Skaggs School of Pharmacy and Pharmaceutical Sciences, University of California, San Diego, La Jolla, California 92093, United States*
**Vivian Hook** − *Skaggs School of Pharmacy and Pharmaceutical Sciences, University of California, San Diego, La Jolla, California 92093, United States*
**Chien-Te Tseng** − *Department of Microbiology and Immunology, University of Texas, Medical Branch, Galveston, Texas 77755-1001, United States*
**Mark Larance** − *Charles Perkins Centre and School of Life and Environmental Sciences, The University of Sydney, Sydney, NSW 2006, Australia;* orcid.org/0000-0002-8579-2267
**Stuart Turville** − *Kirby Institute, University of New South Wales, Sydney, NSW 2052, Australia*

Complete contact information is available at: https://pubs.acs.org/10.1021/acs.jmedchem.1c01494

### Author Contributions

⬡A.S.A. and A.H.T. contributed equally. A.S.A., W.H.G., A.J.O., and R.J.P. initiated and designed the project and managed the consortium. A.S.A. and M.L. performed cell-based assays, cytotoxicity experiments, and proteomics and analyzed the data. A.H.T. and A.S. synthesized gallinamide A (**1**) and analogues **11**−**33** and analyzed the NMR data. A.H.T also performed large scale synthesis of **1** and the alkyne functionalized gallinamide A probe. M.J.B synthesized biotin azide. P.F., M.Y., L.B., D.P, L.L, T.D.M., and V.H. performed the enzymatic assays and analyzed the data. D.S., P.F., and J.H.M. cloned, expressed, and purified SARS-CoV-2 Mpro. A.A. and S.T. performed the *in vitro* SARS-CoV-2 assays on VeroE6, MRC5, and HEK cells and analyzed the data. A.D. and C-T.T. performed the *in vitro* SARS-CoV-2 assays on A549 cells and analyzed the data. A.S.A., A.H.T., W.H.G., A.J.O., and R.J.P. wrote the manuscript and prepared the figures with input from all authors.

### Funding

We would like to acknowledge the National Health and Medical Research Council of Australia for funding (APP1174941). Support for the original discovery and description of gallinamide A is acknowledged from the Fogarty International Center (FIC) through the International Cooperative Biodiversity Group (ICBG) program (U01 TW006634). M.L. is a Cancer Institute New South Wales Future Research Leader Fellow.

### Notes

The authors declare no competing financial interest.

## ■ ACKNOWLEDGMENTS

Figures 1A and 2A were created with BioRender.com. We thank B. Hurst (NIAID) for initial evaluation of gallinamide A in a SARS-CoV-2 assay. The SARS-CoV-2 Mpro expression plasmid was kindly provided to us from Rolf Hilgenfeld, University of Lübeck, Germany. We appreciate support from the UCSD Chancellor's office through an initiative to create a campus wide small molecule resource library. We acknowledge the assistance of Jason Hsu, Vivian Tat, and Rayavara Kempaiah for assistance with tissue culture. We would also like to thank Dr. Luke Dowman for helpful suggestions. We acknowledge Brendan Duggan for technical support with NMR spectroscopy. We thank Sydney Mass Spectrometry for providing instrumentation used in this study.

## ■ ABBREVIATIONS

ACE2, angiotensin-converting enzyme 2; A549/ACE2, adenocarcinomic human alveolar basal epithelial cells over-expressing ACE2; CatB, cathepsin B; CatK, cathepsin K; CatL, cathepsin L; CatS, cathepsin S; CatV, cathepsin V; COVID-19, coronavirus disease 19; CPE, viral cytopathic effects; HEK293T, human embryonic kidney 293T; Mpro, SARS-CoV-2 main protease; MRC5, Medical Research Council cell strain-5; PLpro, SARS-CoV-2 papain-like protease; RBD, receptor-binding domain; S, SARS-CoV-2 homotrimeric spike glycoprotein; SARS-CoV-2, severe acute respiratory syndrome coronavirus 2; TMPRSS2, transmembrane protease serine 2; VeroE6, Vero 76 clone E6 cells

## ■ REFERENCES

(1) World Health Organization. WHO Director-General's opening remarks at the media briefing on COVID-19. 2020.
(2) Krammer, F. SARS-CoV-2 vaccines in development. *Nature* **2020**, *586*, 516−527.
(3) Polack, F. P.; Thomas, S. J.; Kitchin, N.; Absalon, J.; Gurtman, A.; Lockhart, S.; Perez, J. L.; Pérez Marc, G.; Moreira, E. D.; Zerbini, C.; Bailey, R.; Swanson, K. A.; Roychoudhury, S.; Koury, K.; Li, P.; Kalina, W. V.; Cooper, D.; Frenck, R. W.; Hammitt, L. L.; Türeci, Ö.; Nell, H.; Schaefer, A.; Ünal, S.; Tresnan, D. B.; Mather, S.; Dormitzer, P. R.; Şahin, U.; Jansen, K. U.; Gruber, W. C. Safety and efficacy of the BNT162b2 mRNA Covid-19. *N. Engl. J. Med.* **2020**, *383*, 2603−2615.

(4) Voysey, M.; Clemens, S. A. C.; Madhi, S. A.; Weckx, L. Y.; Folegatti, P. M.; Aley, P. K.; Angus, B.; Baillie, V. L.; Barnabas, S. L.; Bhorat, Q. E.; Bibi, S.; Briner, C.; Cicconi, P.; Collins, A. M.; Colin-Jones, R.; Cutland, C. L.; Darton, T. C.; Dheda, K.; Duncan, C. J. A.; Emary, K. R. W.; Ewer, K. J.; Fairlie, L.; Faust, S. N.; Feng, S.; Ferreira, D. M.; Finn, A.; Goodman, A. L.; Green, C. M.; Green, C. A.; Heath, P. T.; Hill, C.; Hill, H.; Hirsch, I.; Hodgson, S. H. C.; Izu, A.; Jackson, S.; Jenkin, D.; Joe, C. C. D.; Kerridge, S.; Koen, A.; Kwatra, G.; Lazarus, R.; Lawrie, A. M.; Lelliott, A.; Libri, V.; Lillie, P. J.; Mallory, R.; Mendes, A. V. A.; Milan, E. P.; Minassian, A. M.; McGregor, A.; Morrison, H.; Mujadidi, Y. F.; Nana, A.; O'Reilly, P. J.; Padayachee, S. D.; Pittella, A.; Plested, E.; Pollock, K. M.; Ramasamy, M. N.; Rhead, S.; Schwarzbold, A. V.; Singh, N.; Smith, A.; Song, R.; Snape, M. D.; Sprinz, E.; Sutherland, R. K.; Tarrant, R.; Thomson, E. C.; Török, M. E.; Toshner, M.; Turner, D. P. J.; Vekemans, J.; Villafana, T. L.; Watson, M. E. E.; Williams, C. J.; Douglas, A. D.; Hill, A. V. S.; Lambe, T.; Gilbert, S. C.; Pollard, A. J. on behalf of the Oxford COVID Vaccine Trial Group. Safety and efficacy of the ChAdOx1 nCoV-19 vaccine (AZD1222) against SARS-CoV-2: an interim analysis of four randomised controlled trials in Brazil, South Africa, and the UK. *Lancet* **2021**, *397*, 99−111.

(5) Poland, G. A.; Ovsyannikova, I. G.; Kennedy, R. B. SARS-CoV-2 immunity: review and applications to phase 3 vaccine candidates. *Lancet* **2020**, *396*, 1595−1606.

(6) Beigel, J. H.; Tomashek, K. M.; Dodd, L. E.; Mehta, A. K.; Zingman, B. S.; Kalil, A. C.; Hohmann, E.; Chu, H. Y.; Luetkemeyer, A.; Kline, S.; Lopez de Castilla, D.; Finberg, R. W.; Dierberg, K.; Tapson, V.; Hsieh, L.; Patterson, T. F.; Paredes, R.; Sweeney, D. A.; Short, W. R.; Touloumi, G.; Lye, D. C.; Ohmagari, N.; Oh, M.-d.; Ruiz-Palacios, G. M.; Benfield, T.; Fätkenheuer, G.; Kortepeter, M. G.; Atmar, R. L.; Creech, C. B.; Lundgren, J.; Babiker, A. G.; Pett, S.; Neaton, J. D.; Burgess, T. H.; Bonnett, T.; Green, M.; Makowski, M.; Osinusi, A.; Nayak, S.; Lane, H. C. Remdesivir for the treatment of Covid-19 — final report. *N. Engl. J. Med.* **2020**, *383*, 1813−1826.

(7) Wang, Y.; Zhang, D.; Du, G.; Du, R.; Zhao, J.; Jin, Y.; Fu, S.; Gao, L.; Cheng, Z.; Lu, Q.; Hu, Y.; Luo, G.; Wang, K.; Lu, Y.; Li, H.; Wang, S.; Ruan, S.; Yang, C.; Mei, C.; Wang, Y.; Ding, D.; Wu, F.; Tang, X.; Ye, X.; Ye, Y.; Liu, B.; Yang, J.; Yin, W.; Wang, A.; Fan, G.; Zhou, F.; Liu, Z.; Gu, X.; Xu, J.; Shang, L.; Zhang, Y.; Cao, L.; Guo, T.; Wan, Y.; Qin, H.; Jiang, Y.; Jaki, T.; Hayden, F. G.; Horby, P. W.; Cao, B.; Wang, C. Remdesivir in adults with severe COVID-19: a randomised, double-blind, placebo-controlled, multicentre trial. *Lancet* **2020**, *395*, 1569−1578.

(8) Dyer, O. Covid-19: Remdesivir has little or no impact on survival, WHO trial shows. *BMJ.* **2020**, *371*, m405.

(9) Boulware, D. R.; Pullen, M. F.; Bangdiwala, A. S.; Pastick, K. A.; Lofgren, S. M.; Okafor, E. C.; Skipper, C. P.; Nascene, A. A.; Nicol, M. R.; Abassi, M.; Engen, N. W.; Cheng, M. P.; LaBar, D.; Lother, S. A.; MacKenzie, L. J.; Drobot, G.; Marten, N.; Zarychanski, R.; Kelly, L. E.; Schwartz, I. S.; McDonald, E. G.; Rajasingham, R.; Lee, T. C.; Hullsiek, K. H. A Randomized trial of hydroxychloroquine as postexposure prophylaxis for Covid-19. *N. Engl. J. Med.* **2020**, *383*, 517−525.

(10) Skipper, C. P.; Pastick, K. A.; Engen, N. W.; Bangdiwala, A. S.; Abassi, M.; Lofgren, S. M.; Williams, D. A.; Okafor, E. C.; Pullen, M. F.; Nicol, M. R.; Nascene, A. A.; Hullsiek, K. H.; Cheng, M. P.; Luke, D.; Lother, S. A.; MacKenzie, L. J.; Drobot, G.; Kelly, L. E.; Schwartz, I. S.; Zarychanski, R.; McDonald, E. G.; Lee, T. C.; Rajasingham, R.; Boulware, D. R. Hydroxychloroquine in non-hospitalized adults with early COVID-19: a randomized trial. *Ann. Intern. Med.* **2020**, *173*, 623−631.

(11) Cavalcanti, A. B.; Zampieri, F. G.; Rosa, R. G.; Azevedo, L. C. P.; Veiga, V. C.; Avezum, A.; Damiani, L. P.; Marcadenti, A.; Kawano-Dourado, L.; Lisboa, T.; Junqueira, D. L. M.; de Barros e Silva, P. G. M.; Tramujas, L.; Abreu-Silva, E. O.; Laranjeira, L. N.; Soares, A. T.; Echenique, L. S.; Pereira, A. J.; Freitas, F. G. R.; Gebara, O. C. E.; Dantas, V. C. S.; Furtado, R. H. M.; Milan, E. P.; Golin, N. A.; Cardoso, F. F.; Maia, I. S.; Hoffmann Filho, C. R.; Kormann, A. P. M.; Amazonas, R. B.; Bocchi de Oliveira, M. F.; Serpa-Neto, A.; Falavigna, M.; Lopes, R. D.; Machado, F. R.; Berwanger, O. Hydroxychloroquine with or without azithromycin in mild-to-moderate Covid-19. *N. Engl. J. Med.* **2020**, *383*, 2041−2052.

(12) Horby, P. W.; Mafham, M.; Bell, J. L.; Linsell, L.; Staplin, N.; Emberson, J.; Palfreeman, A.; Raw, J.; Elmahi, E.; Prudon, B.; Green, C.; Carley, S.; Chadwick, D.; Davies, M.; Wise, M. P.; Baillie, J. K.; Chappell, L. C.; Faust, S. N.; Jaki, T.; Jefferey, K.; Lim, W. S.; Montgomery, A.; Rowan, K.; Juszczak, E.; Haynes, R.; Landray, M. J. Lopinavir-ritonavir in patients admitted to hospital with COVID-19 (RECOVERY): a randomised, controlled, open-label, platform trial. *Lancet* **2020**, *396*, 1345−1352.

(13) Cao, B.; Wang, Y.; Wen, D.; Liu, W.; Wang, J.; Fan, G.; Ruan, L.; Song, B.; Cai, Y.; Wei, M.; Li, X.; Xia, J.; Chen, N.; Xiang, J.; Yu, T.; Bai, T.; Xie, X.; Zhang, L.; Li, C.; Yuan, Y.; Chen, H.; Li, H.; Huang, H.; Tu, S.; Gong, F.; Liu, Y.; Wei, Y.; Dong, C.; Zhou, F.; Gu, X.; Xu, J.; Liu, Z.; Zhang, Y.; Li, H.; Shang, L.; Wang, K.; Li, K.; Zhou, X.; Dong, X.; Qu, Z.; Lu, S.; Hu, X.; Ruan, S.; Luo, S.; Wu, J.; Peng, L.; Cheng, F.; Pan, L.; Zou, J.; Jia, C.; Wang, J.; Liu, X.; Wang, S.; Wu, X.; Ge, Q.; He, J.; Zhan, H.; Qiu, F.; Guo, L.; Huang, C.; Jaki, T.; Hayden, F. G.; Horby, P. W.; Zhang, D.; Wang, C. A trial of lopinavir−ritonavir in adults hospitalized with severe Covid-19. *N. Engl. J. Med.* **2020**, *382*, 1787−1799.

(14) Peiffer-Smadja, N.; Yazdanpanah, Y. Nebulised interferon beta-1a for patients with COVID-19. *Lancet Respir. Med.* **2021**, *9*, 122−123.

(15) Schreiber, G.The role of type I interferons in the pathogenesis and treatment of COVID-19. *Front. Immunol.***2020**, *11*, 595739.

(16) The RECOVERY Collaborative Group. Dexamethasone in hospitalized patients with Covid-19. *N. Engl. J. Med.* **2021**, *384*, 693−704.

(17) Molina, J. M.; Capitant, C.; Spire, B.; Pialoux, G.; Cotte, L.; Charreau, I.; Tremblay, C.; Le Gall, J. M.; Cua, E.; Pasquet, A.; Raffi, F.; Pintado, C.; Chidiac, C.; Chas, J.; Charbonneau, P.; Delaugerre, C.; Suzan-Monti, M.; Loze, B.; Fonsart, J.; Peytavin, G.; Cheret, A.; Timsit, J.; Girard, G.; Lorente, N.; Préau, M.; Rooney, J. F.; Wainberg, M. A.; Thompson, D.; Rozenbaum, W.; Doré, V.; Marchand, L.; Simon, M. C.; Etien, N.; Aboulker, J. P.; Meyer, L.; Delfraissy, J. F. On-demand preexposure prophylaxis in men at high risk for HIV-1 infection. *N. Engl. J. Med.* **2015**, *373*, 2237−2246.

(18) Shang, J.; Wan, Y.; Luo, C.; Ye, G.; Geng, Q.; Auerbach, A.; Li, F. Cell entry mechanisms of SARS-CoV-2. *Proc. Natl. Acad. Sci. U. S. A.* **2020**, *117*, 11727−11734.

(19) Hoffmann, M.; Kleine-Weber, H.; Schroeder, S.; Krüger, N.; Herrler, T.; Erichsen, S.; Schiergens, T. S.; Herrler, G.; Wu, N.-H.; Nitsche, A.; Müller, M. A.; Drosten, C.; Pöhlmann, S. SARS-CoV-2 cell entry depends on ACE2 and TMPRSS2 and is blocked by a clinically proven protease inhibitor. *Cell* **2020**, *181*, 271−280.

(20) Letko, M.; Marzi, A.; Munster, V. Functional assessment of cell entry and receptor usage for SARS-CoV-2 and other lineage B betacoronaviruses. *Nat. Microbiol.* **2020**, *5*, 562−569.

(21) Wang, K.; Chen, W.; Zhang, Z.; Deng, Y.; Lian, J.-Q.; Du, P.; Wei, D.; Zhang, Y.; Sun, X.-X.; Gong, L.; Yang, X.; He, L.; Zhang, L.; Yang, Z.; Geng, J.-J.; Chen, R.; Zhang, H.; Wang, B.; Zhu, Y.-M.; Nan, G.; Jiang, J.-L.; Li, L.; Wu, J.; Lin, P.; Huang, W.; Xie, L.; Zheng, Z.-H.; Zhang, K.; Miao, J.-L.; Cui, H.-Y.; Huang, M.; Zhang, J.; Fu, L.; Yang, X.-M.; Zhao, Z.; Sun, S.; Gu, H.; Wang, Z.; Wang, C.-F.; Lu, Y.; Liu, Y.-Y.; Wang, Q.-Y.; Bian, H.; Zhu, P.; Chen, Z.-N. CD147-spike protein is a novel route for SARS-CoV-2 infection to host cells. *Signal Transduct. Target. Ther.* **2020**, *5*, 283.

(22) Pišlar, A.; Mitrović, A.; Sabotič, J.; Pečar Fonović, U.; Perišić Nanut, M.; Jakoš, T.; Senjor, E.; Kos, J. The role of cysteine peptidases in coronavirus cell entry and replication: the therapeutic potential of cathepsin inhibitors. *PLoS Pathog.* **2020**, *16*, e1009013.

(23) Mellott, D. M.; Tseng, C.-T.; Drelich, A.; Fajtová, P.; Chenna, B. C.; Kostomiris, D. H.; Hsu, J.; Zhu, J.; Taylor, Z. W.; Kocurek, K. I.; Tat, V.; Katzfuss, A.; Li, L.; Giardini, M. A.; Skinner, D.; Hirata, K.; Yoon, M. C.; Beck, S.; Carlin, A. F.; Clark, A. E.; Beretta, L.; Maneval, D.; Hook, V.; Frueh, F.; Hurst, B. L.; Wang, H.; Raushel, F. M.; O'Donoghue, A. J.; de Siqueira-Neto, J. L.; Meek, T. D.;



https://doi.org/10.1021/acs.jmedchem.1c01494
J. Med. Chem. XXXX, XXX, XXX−XXX

McKerrow, J. H. A clinical-stage cysteine protease inhibitor blocks SARS-CoV-2 infection of human and monkey cells. *ACS Chem. Biol.* **2021**, *16*, 642−650.
(24) Zhao, M.-M.; Yang, W.-L.; Yang, F.-Y.; Zhang, L.; Huang, W.-J.; Hou, W.; Fan, C.-F.; Jin, R.-H.; Feng, Y.-M.; Wang, Y.-C.; Yang, J.-K. Cathepsin L plays a key role in SARS-CoV-2 infection in humans and humanized mice and is a promising target for new drug development. *Sig. Transduct. Target. Ther.* **2021**, *6*, 134.
(25) Gerber, A.; Welte, T.; Ansorge, S.; Bühling, F. In *Cellular Peptidases in Immune Functions and Diseases 2*, Langner, J., Ansorge, S., Eds.; Springer US: Boston, MA, 2002; pp 287−292.
(26) Coomes, E. A.; Haghbayan, H. Interleukin-6 in Covid-19: a systematic review and meta-analysis. *Rev. Med. Virol.* **2020**, *30*, 1−9.
(27) Liu, T.; Luo, S.; Libby, P.; Shi, G.-P. Cathepsin L-selective inhibitors: a potentially promising treatment for COVID-19 patients. *Pharmacol. Ther.* **2020**, *213*, 107587.
(28) Hoffmann, M.; Schroeder, S.; Kleine-Weber, H.; Müller, M. A.; Drosten, C.; Pöhlmann, S. Nafamostat mesylate blocks activation of SARS-CoV-2: new treatment option for COVID-19. *Antimicrob. Agents Chemother.* **2020**, *64*, e00754.
(29) Shin, D.; Mukherjee, R.; Grewe, D.; Bojkova, D.; Baek, K.; Bhattacharya, A.; Schulz, L.; Widera, M.; Mehdipour, A. R.; Tascher, G.; Geurink, P. P.; Wilhelm, A.; van der Heden van Noort, G. J.; Ovaa, H.; Müller, S.; Knobeloch, K.-P.; Rajalingam, K.; Schulman, B. A.; Cinatl, J.; Hummer, G.; Ciesek, S.; Dikic, I. Papain-like protease regulates SARS-CoV-2 viral spread and innate immunity. *Nature* **2020**, *587*, 657−662.
(30) Zhang, L.; Lin, D.; Sun, X.; Curth, U.; Drosten, C.; Sauerhering, L.; Becker, S.; Rox, K.; Hilgenfeld, R. Crystal structure of SARS-CoV-2 main protease provides a basis for design of improved α-ketoamide inhibitors. *Science* **2020**, *368*, 409−412.
(31) Jin, Z.; Du, X.; Xu, Y.; Deng, Y.; Liu, M.; Zhao, Y.; Zhang, B.; Li, X.; Zhang, L.; Peng, C.; Duan, Y.; Yu, J.; Wang, L.; Yang, K.; Liu, F.; Jiang, R.; Yang, X.; You, T.; Liu, X.; Yang, X.; Bai, F.; Liu, H.; Liu, X.; Guddat, L. W.; Xu, W.; Xiao, G.; Qin, C.; Shi, Z.; Jiang, H.; Rao, Z.; Yang, H. Structure of Mpro from SARS-CoV-2 and discovery of its inhibitors. *Nature* **2020**, *582*, 289−293.
(32) Dai, W.; Zhang, B.; Jiang, X.-M.; Su, H.; Li, J.; Zhao, Y.; Xie, X.; Jin, Z.; Peng, J.; Liu, F.; Li, C.; Li, Y.; Bai, F.; Wang, H.; Cheng, X.; Cen, X.; Hu, S.; Yang, X.; Wang, J.; Liu, X.; Xiao, G.; Jiang, H.; Rao, Z.; Zhang, L.-K.; Xu, Y.; Yang, H.; Liu, H. Structure-based design of antiviral drug candidates targeting the SARS-CoV-2 main protease. *Science* **2020**, *368*, 1331−1335.
(33) Linington, R. G.; Clark, B. R.; Trimble, E. E.; Almanza, A.; Urena, L.-D.; Kyle, D. E.; Gerwick, W. H. Antimalarial peptides from marine cyanobacteria: isolation and structural elucidation of gallinamide A. *J. Nat. Prod.* **2009**, *72*, 14−17.
(34) Taori, K.; Liu, Y.; Paul, V. J.; Luesch, H. Combinatorial strategies by marine cyanobacteria: symplostatin 4, an antimitotic natural dolastatin 10/15 hybrid that synergizes with the coproduced HDAC inhibitor largazole. *ChemBioChem* **2009**, *10*, 1634−1639.
(35) Stolze, S. C.; Deu, E.; Kaschani, F.; Li, N.; Florea, B. I.; Richau, K. H.; Colby, T.; van der Hoorn, R. A. L.; Overkleeft, H. S.; Bogyo, M.; Kaiser, M. The antimalarial natural product symplostatin 4 is a nanomolar inhibitor of the food vacuole falcipains. *Chem. Biol.* **2012**, *19*, 1546−1555.
(36) Conroy, T.; Guo, J. T.; Elias, N.; Cergol, K. M.; Gut, J.; Legac, J.; Khatoon, L.; Liu, Y.; McGowan, S.; Rosenthal, P. J.; Hunt, N. H.; Payne, R. J. Synthesis of gallinamide A analogues as potent falcipain inhibitors and antimalarials. *J. Med. Chem.* **2014**, *57*, 10557−10563.
(37) Boudreau, P. D.; Miller, B. W.; McCall, L.-I.; Almaliti, J.; Reher, R.; Hirata, K.; Le, T.; Siqueira-Neto, J. L.; Hook, V.; Gerwick, W. H. Design of gallinamide A analogs as potent inhibitors of the cysteine proteases human cathepsin L and Trypanosoma cruzi cruzain. *J. Med. Chem.* **2019**, *62*, 9026−9044.
(38) Miller, B.; Friedman, A. J.; Choi, H.; Hogan, J.; McCammon, J. A.; Hook, V.; Gerwick, W. H. The marine cyanobacterial metabolite gallinamide A is a potent and selective inhibitor of human cathepsin L. *J. Nat. Prod.* **2014**, *77*, 92−99.
(39) Stoye, A.; Juillard, A.; Tang, A. H.; Legac, J.; Gut, J.; White, K. L.; Charman, S. A.; Rosenthal, P. J.; Grau, G. E. R.; Hunt, N. H.; Payne, R. J. Falcipain inhibitors based on the natural product gallinamide A are potent in vitro and in vivo antimalarials. *J. Med. Chem.* **2019**, *62*, 5562−5578.
(40) Sacco, M. D.; Ma, C.; Lagarias, P.; Gao, A.; Townsend, J. A.; Meng, X.; Dube, P.; Zhang, X.; Hu, Y.; Kitamura, N.; Hurst, B.; Tarbet, B.; Marty, M. T.; Kolocouris, A.; Xiang, Y.; Chen, Y.; Wang, J. Structure and inhibition of the SARS-CoV-2 main protease reveal strategy for developing dual inhibitors against $M^{pro}$ and cathepsin L. *Sci. Adv.* **2020**, *6*, eabe0751.
(41) Steuten, K.; Kim, H.; Widen, J. C.; Babin, B. M.; Onguka, O.; Lovell, S.; Bolgi, O.; Cerikan, B.; Neufeldt, C. J.; Cortese, M.; Muir, R. K.; Bennett, J. M.; Geiss-Friedlander, R.; Peters, C.; Bartenschlager, R.; Bogyo, M. Challenges for targeting SARS-CoV-2 proteases as a therapeutic strategy for COVID-19. *ACS Infect. Dis.* **2021**, *7*, 1457−1468.
(42) Montaser, M.; Lalmanach, G.; Mach, L. CA-074, but not its methyl ester CA-074Me, is a selective inhibitor of cathepsin B within living cells. *Biol. Chem.* **2002**, *383*, 1305−1308.
(43) Zhang, L.; Jackson, C. B.; Mou, H.; Ojha, A.; Peng, H.; Quinlan, B. D.; Rangarajan, E. S.; Pan, A.; Vanderheiden, A.; Suthar, M. S.; Li, W.; Izard, T.; Rader, C.; Farzan, M.; Choe, H. SARS-CoV-2 spike-protein D614G mutation increases virion spike density and infectivity. *Nat. Commun.* **2020**, *11*, 6013.
(44) Bertram, S.; Dijkman, R.; Habjan, M.; Heurich, A.; Gierer, S.; Glowacka, I.; Welsch, K.; Winkler, M.; Schneider, H.; Hofmann-Winkler, H.; Thiel, V.; Pohlmann, S. TMPRSS2 activates the human coronavirus 229E for cathepsin-independent host cell entry and is expressed in viral target cells in the respiratory epithelium. *J. Virol.* **2013**, *87*, 6150−6160.
(45) Zhou, N.; Pan, T.; Zhang, J.; Li, Q.; Zhang, X.; Bai, C.; Huang, F.; Peng, T.; Zhang, J.; Liu, C.; Tao, L.; Zhang, H. Glycopeptide antibiotics potently inhibit cathepsin L in the late endosome/lysosome and block the entry of Ebola virus, Middle East Respiratory Syndrome Coronavirus (MERS-CoV), and Severe Acute Respiratory Syndrome Coronavirus (SARS-CoV). *J. Biol. Chem.* **2016**, *291*, 9218−9232.
(46) Shah, P. P.; Wang, T.; Kaletsky, R. L.; Myers, M. C.; Purvis, J. E.; Jing, H.; Huryn, D. M.; Greenbaum, D. C.; Smith, A. B., 3rd; Bates, P.; Diamond, S. L. A small-molecule oxocarbazate inhibitor of human cathepsin L blocks severe acute respiratory syndrome and Ebola pseudotype virus infection into human embryonic kidney 293T cells. *Mol. Pharmacol.* **2010**, *78*, 319−324.
(47) Nie, X.; Qian, L.; Sun, R.; Huang, B.; Dong, X.; Xiao, Q.; Zhang, Q.; Lu, T.; Yue, L.; Chen, S.; Li, X.; Sun, Y.; Li, L.; Xu, L.; Li, Y.; Yang, M.; Xue, Z.; Liang, S.; Ding, X.; Yuan, C.; Peng, L.; Liu, W.; Yi, X.; Lyu, M.; Xiao, G.; Xu, X.; Ge, W.; He, J.; Fan, J.; Wu, J.; Luo, M.; Chang, X.; Pan, H.; Cai, X.; Zhou, J.; Yu, J.; Gao, H.; Xie, M.; Wang, S.; Ruan, G.; Chen, H.; Su, H.; Mei, H.; Luo, D.; Zhao, D.; Xu, F.; Li, Y.; Zhu, Y.; Xia, J.; Hu, Y.; Guo, T. Multi-organ proteomic landscape of COVID-19 autopsies. *Cell* **2021**, *184*, 775−791.
(48) Newman, D. J.; Cragg, G. M. Natural products as sources of new drugs over the nearly four decades from 01/1981 to 09/2019. *J. Nat. Prod.* **2020**, *83*, 770−803.
(49) Christy, M. P.; Uekusa, Y.; Gerwick, L.; Gerwick, W. H. Natural products with potential to treat RNA virus pathogens including SARS-CoV-2. *J. Nat. Prod.* **2021**, *84*, 161−182.
(50) Sudhan, D. R.; Siemann, D. W. Cathepsin L targeting in cancer treatment. *Pharmacol. Ther.* **2015**, *155*, 105−116.
(51) Schedel, J.; Seemayer, C. A.; Pap, T.; Neidhart, M.; Kuchen, S.; Michel, B. A.; Gay, R. E.; Müller-Ladner, U.; Gay, S.; Zacharias, W. Targeting cathepsin L (CL) by specific ribozymes decreases CL protein synthesis and cartilage destruction in rheumatoid arthritis. *Gene Ther.* **2004**, *11*, 1040−1047.
(52) Garsen, M.; Rops, A. L.; Dijkman, H.; Willemsen, B.; van Kuppevelt, T. H.; Russel, F. G.; Rabelink, T. J.; Berden, J. H.; Reinheckel, T.; van der Vlag, J. Cathepsin L is crucial for the


https://doi.org/10.1021/acs.jmedchem.1c01494
J. Med. Chem. XXXX, XXX, XXX−XXX

development of early experimental diabetic nephropathy. *Kidney Int.* **2016**, *90*, 1012−1022.
(53) Li, Y. Y.; Fang, J.; Ao, G. Z. Cathepsin B and L inhibitors: a patent review (2010 - present). *Expert Opin. Ther. Pat.* **2017**, *27*, 643−656.
(54) Roth, W.; Deussing, J.; Botchkarev, V. A.; Pauly-Evers, M.; Saftig, P.; Hafner, A.; Schmidt, P.; Schmahl, W.; Scherer, J.; Anton-Lamprecht, I.; Von Figura, K.; Paus, R.; Peters, C. Cathepsin L deficiency as molecular defect of furless: hyperproliferation of keratinocytes and pertubation of hair follicle cycling. *FASEB J.* **2000**, *14*, 2075−2086.
(55) Potts, W.; Bowyer, J.; Jones, H.; Tucker, D.; Freemont, A. J.; Millest, A.; Martin, C.; Vernon, W.; Neerunjun, D.; Slynn, G.; Harper, F.; Maciewicz, R. Cathepsin L-deficient mice exhibit abnormal skin and bone development and show increased resistance to osteoporosis following ovariectomy. *Int. J. Exp. Pathol.* **2004**, *85*, 85−96.
(56) Petermann, I.; Mayer, C.; Stypmann, J.; Biniossek, M. L.; Tobin, D. J.; Engelen, M. A.; Dandekar, T.; Grune, T.; Schild, L.; Peters, C.; Reinheckel, T. Lysosomal, cytoskeletal, and metabolic alterations in cardiomyopathy of cathepsin L knockout mice. *FASEB J.* **2006**, *20*, 1266−1268.
(57) Xu, X.; Greenland, J.; Baluk, P.; Adams, A.; Bose, O.; McDonald, D. M.; Caughey, G. H. Cathepsin L protects mice from mycoplasmal infection and is essential for airway lymphangiogenesis. *Am. J. Respir. Cell Mol. Biol.* **2013**, *49*, 437−444.
(58) McKerrow, J. H. Update on drug development targeting parasite cysteine proteases. *PLoS Neglected Trop. Dis.* **2018**, *12*, e0005850.
(59) Koch, J.; Uckeley, Z. M.; Doldan, P.; Stanifer, M.; Boulant, S.; Lozach, P.-Y. TMPRSS2 expression dictates the entry route used by SARS-CoV-2 to infect host cells. *EMBO J.* **2021**, *40*, e107821.
(60) Ou, T.; Mou, H.; Zhang, L.; Ojha, A.; Choe, H.; Farzan, M. Hydroxychloroquine-mediated inhibition of SARS-CoV-2 entry is attenuated by TMPRSS2. *PLoS Pathog.* **2021**, *17*, e1009212.
(61) Puelles, V. G.; Lütgehetmann, M.; Lindenmeyer, M. T.; Sperhake, J. P.; Wong, M. N.; Allweiss, L.; Chilla, S.; Heinemann, A.; Wanner, N.; Liu, S.; Braun, F.; Lu, S.; Pfefferle, S.; Schröder, A. S.; Edler, C.; Gross, O.; Glatzel, M.; Wichmann, D.; Wiech, T.; Kluge, S.; Pueschel, K.; Aepfelbacher, M.; Huber, T. B. Multiorgan and renal tropism of SARS-CoV-2. *N. Engl. J. Med.* **2020**, *383*, 590−592.
(62) Lukassen, S.; Chua, R. L.; Trefzer, T.; Kahn, N. C.; Schneider, M. A.; Muley, T.; Winter, H.; Meister, M.; Veith, C.; Boots, A. W.; Hennig, B. P.; Kreuter, M.; Conrad, C.; Eils, R. SARS-CoV-2 receptor ACE2 and TMPRSS2 are primarily expressed in bronchial transient secretory cells. *EMBO J.* **2020**, *39*, e105114.
(63) Tonge, P. J. Quantifying the interactions between biomolecules: guidelines for assay design and data analysis. *ACS Infect. Dis.* **2019**, *5*, 796−808.
(64) Follenzi, A.; Battaglia, M.; Lombardo, A.; Annoni, A.; Roncarolo, M. G.; Naldini, L. Targeting lentiviral vector expression to hepatocytes limits transgene-specific immune response and establishes long-term expression of human antihemophilic factor IX in mice. *Blood* **2004**, *103*, 3700−3709.
(65) Aggarwal, A.; Iemma, T. L.; Shih, I.; Newsome, T. P.; McAllery, S.; Cunningham, A. L.; Turville, S. G. Mobilization of HIV spread by diaphanous 2 dependent filopodia in infected dendritic cells. *PLoS Pathog.* **2012**, *8*, e1002762.
(66) Tea, F.; Ospina Stella, A.; Aggarwal, A.; Ross Darley, D.; Pilli, D.; Vitale, D.; Merheb, V.; Lee, F. X. Z.; Cunningham, P.; Walker, G. J.; Fichter, C.; Brown, D. A.; Rawlinson, W. D.; Isaacs, S. R.; Mathivanan, V.; Hoffmann, M.; Pöhlman, S.; Mazigi, O.; Christ, D.; Rockett, R. J.; Sintchenko, V.; Hoad, V. C.; Irving, D. O.; Dore, G. J.; Gosbell, I. B.; Kelleher, A. D.; Matthews, G. V.; Brilot, F.; Turville, S. G. SARS-CoV-2 neutralizing antibodies: Longevity, breadth, and evasion by emerging viral variants. *PLoS Med.* **2021**, *18*, e1003656.
(67) Darabedian, N.; Pratt, M. R. Identifying potentially O-GlcNAcylated proteins using metabolic labeling, bioorthogonal enrichment, and Western blotting. *Methods Enzymol.* **2019**, *622*, 293−307.
(68) Harney, D. J.; Cielesh, M.; Chu, R.; Cooke, K. C.; James, D. E.; Stöckli, J.; Larance, M. Proteomics analysis of adipose depots after intermittent fasting reveals visceral fat preservation mechanisms. *Cell Rep.* **2021**, *34*, 108804.
(69) Walker, G. J.; Clifford, V.; Bansal, N.; Stella, A. O.; Turville, S.; Stelzer-Braid, S.; Klein, L. D.; Rawlinson, W. SARS-CoV-2 in human milk is inactivated by Holder pasteurisation but not cold storage. *J. Paediatr. Child Health* **2020**, *56*, 1872−1874.
(70) Aggarwal, A.; Hitchen, T. L.; Ootes, L.; McAllery, S.; Wong, A.; Nguyen, K.; McCluskey, A.; Robinson, P. J.; Turville, S. G. HIV infection is influenced by dynamin at 3 independent points in the viral life cycle. *Traffic* **2017**, *18*, 392−410.
(71) Chou, T. C. Preclinical versus clinical drug combination studies. *Leuk. Lymphoma* **2008**, *49*, 2059−2080.
(72) Chou, T. C. Drug combination studies and their synergy quantification using the Chou-Talalay method. *Cancer Res.* **2010**, *70*, 440−446.
(73) Chou, T. C. Theoretical basis, experimental design, and computerized simulation of synergism and antagonism in drug combination studies. *Pharmacol. Rev.* **2006**, *58*, 621−681.
(74) Chou, T. C.; Talalay, P. Quantitative analysis of dose-effect relationships: the combined effects of multiple drugs or enzyme inhibitors. *Adv. Enzyme Regul.* **1984**, *22*, 27−55.


https://doi.org/10.1021/acs.jmedchem.1c01494
J. Med. Chem. XXXX, XXX, XXX−XXX